

Mathematical Modelling and Analysis of the Brassinosteroid and Gibberellin Signalling Pathways and their Interactions

Henry R. Allen*, Mariya Ptashnyk*,†

July 16, 2018

Abstract

The plant hormones brassinosteroid (BR) and gibberellin (GA) have important roles in a wide range of processes involved in plant growth and development. In this paper we derive and analyse new mathematical models for the BR signalling pathway and for the crosstalk between the BR and GA signalling pathways. To analyse the effects of spatial heterogeneity of the signalling processes, along with spatially-homogeneous ODE models we derive coupled PDE-ODE systems modelling the temporal and spatial dynamics of molecules involved in the signalling pathways. The values of the parameters in the model for the BR signalling pathway are determined using experimental data on the gene expression of BR biosynthetic enzymes. The stability of steady state solutions of our mathematical model, shown for a wide range of parameters, can be related to the BR homeostasis which is essential for proper function of plant cells. Solutions of the mathematical model for the BR signalling pathway can exhibit oscillatory behaviour only for relatively large values of parameters associated with transcription factor brassinazole-resistant1's (BZR) phosphorylation state, suggesting that this process may be important in governing the stability of signalling processes. Comparison between ODE and PDE-ODE models demonstrates distinct spatial distribution in the level of BR in the cell cytoplasm, however the spatial heterogeneity has significant effect on the dynamics of the averaged solutions only in the case when we have oscillations in solutions for at least one of the models, i.e. for possibly biologically not relevant parameter values. Our results for the crosstalk model suggest that the interaction between transcription factors BZR and DELLA exerts more influence on the dynamics of the signalling pathways than BZR-mediated biosynthesis of GA, suggesting that the interaction between transcription factors may constitute the principal mechanism of the crosstalk between the BR and GA signalling pathways. In general, perturbations in the GA signalling pathway have larger effects on the dynamics of components of the BR signalling pathway than perturbations in the BR signalling pathway on the dynamics of the GA pathway. The perturbation in the crosstalk mechanism also has a larger effect on the dynamics of the BR pathway than of the GA pathway. Large changes in the dynamics of the GA signalling processes can be observed only in the case where there are disturbances in both the BR signalling pathway and the crosstalk mechanism. Those results highlight the robustness of the GA signalling pathway.

Key words. plant modelling; hormone crosstalk signalling; homeostasis in plants; stability analysis and Hopf bifurcation; PDE-ODE systems

AMS subject classification. 34Cxx, 35Q92, 65Nxx, 92Bxx, 92Cxx

1 Introduction

The sessile nature of plant life highlights the importance of efficient regulatory mechanisms allowing plants to respond to environmental stimuli and to adapt to changing environmental conditions. Plants have developed a set of highly integrated signalling pathways. Plant hormones, e.g. auxin, gibberellin, cytokinin, brassinosteroids, ethylene, are key signalling molecules and their activities depend on the cellular context and interactions between them.

*Department of Mathematics, Fulton Building, University of Dundee, Dundee, United Kingdom, DD1 4HN

†Corresponding Author

The family of steroidal plant hormones brassinosteroids (BRs) is responsible for the regulation and control of a wide range of essential processes including responses to stresses [7, 23], photomorphogenesis [8, 67], root growth [38], and stomatal development [27]. Over the last 47 years, the effects of brassinosteroids on plant cells and plants as a whole, as well as their signalling pathways have been studied in detail [14]. In particular the signalling pathway of brassinolide (BL), the most biologically active of the discovered BRs, has been examined in great detail, and is now one of the most understood pathways in plant biology [8, 13, 28, 30, 44, 63, 64, 66, 67]. BR signalling functions by controlling the expression of various genes regulating developmental processes, of which 1000s have been identified [49], including several genes which regulate the production of proteins that act as enzymes during BR biosynthesis [50]. To ensure controlled growth, homeostasis of BRs in plant tissue is carefully maintained by negative feedback in the BR signalling pathway [50]. Absence of BRs and/or perturbed BR signalling have also been linked to many growth defects, including dwarfism and male sterility [12, 15].

Gibberellins (GAs) are another family of plant hormones involved in many developmental processes in plants, including seed germination, stem elongation, leaf expansion, trichome development, pollen maturation and the induction of flowering [2, 17]. There are over 130 categorized gibberellins, a few of which are bioactive molecules, the most common being GA_1 , GA_3 and GA_4 [65].

Along with detailed information on individual plant hormone signal transduction pathways, their target genes, and their effects, it is now also known that interactions between various molecules involved in different signalling pathways have an effect on physiological phenomena in plants [6, 8]. For example both auxin and brassinosteroids play a role in the patterning of vascular shoot bundles [25], as well as exhibiting some cross-regulation of biosynthesis via the BRX gene [43]. The GA signalling pathway exhibits a high level of interaction with the BR signalling pathway regulating growth [15, 54] and responses to stresses [2, 7] among others. The interactions between different signalling pathways are called crosstalks, and the investigation of their mechanisms is key to better understand plant hormonal responses to external stimuli [4, 8, 23, 66]. Despite the need for better understanding of the mechanisms of crosstalk between hormone signalling pathways, it is hard to obtain experimentally quantitative data on the dynamics of all molecules involved in the signalling pathways and interactions between them. For example, it is very difficult to measure the dynamics of hormones such as BR in real time, in part due to their occurring naturally at extremely low levels. Therefore development of accurate mathematical models of hormone activity can help to analyse and better understand interactions between signalling pathways and their impact on plant growth and development. Hence, the main aim of this paper is to derive and analyse novel mathematical models for the BR signalling pathway, and the crosstalk between the BR and GA signalling pathways.

Along with many modelling results for the gibberellin and auxin signalling pathways [22, 34, 35, 36, 37], only a few models can be found for BR-related signalling processes. A logic model for the activation states of the components of the BR and auxin signalling pathways and their interactions was derived in [43], and provided a qualitative description of the dynamics of the BR pathway. In a simple model for BR-mediated root growth, proposed in [58], the growth dynamics is assumed to be dependent on the quantity of receptor-bound BL, which was considered to be constant. A system of ordinary differential equations was considered to describe the dynamics of BR-regulated transcription factor BES1 (BRI1-EMS SUPPRESSOR 1) and its interactions with R2R3-MYB transcription factor BRAVO, related to division of plant stem cells [19, 60]. To our knowledge there are no previous results on mathematical modelling of the crosstalk between BR and GA signalling pathways.

In our mathematical model for the BR signalling pathway, we consider the dynamics of BR, free and bound receptors, inhibitors, and phosphorylated and dephosphorylated transcription factors, not considered in previous models. The spatially homogeneous dynamics of the molecules involved in the signalling pathway that we consider are modelled by a system of six ordinary differential equations (ODEs). To analyse the effect of spatial heterogeneity of the signalling processes on the dynamics of BR, we derive a coupled model composed of partial differential equations (PDEs) for BR, inhibitor,

and phosphorylated transcription factor, ODEs for receptors, defined on the cell membrane, and the ODE for dephosphorylated transcription factors, localised in the cell nucleus. Along with spatial distribution of the concentration of BR in the cell cytoplasm, we observe similar dynamics for solutions of the ODE and averaged solutions of the PDE-ODE models when those solutions converge to a steady state as $t \rightarrow \infty$. However spatial heterogeneity has significant effect in the case when at least one of the two models has periodic solutions, which is determined for possibly biologically not relevant parameter values.

To model the crosstalk between BR and GA signalling pathways we first rigorously derive a reduced model for the GA signalling pathway from the full GA signalling pathway model proposed in [36]. Then we couple the model for the BR signalling pathway with the reduced model for GA signalling pathway by considering three different interaction mechanisms between BR and GA pathways. By analysing the effect of different interaction mechanisms on the dynamics of molecules involved in the signalling processes, we determine that one of these mechanisms has a more significant effect on the dynamics of the signalling pathways than the other mechanisms. Similar to the BR signalling pathway model, we also consider the influence of spatial heterogeneity of the signalling processes on the dynamics of solutions of the BR-GA crosstalk model. Using the mathematical models developed here, we analyse how interactions between the BR and GA signalling pathways depend on the model parameters and the strength of interaction mechanisms. We observed that, in general, parameter changes in both pathways have a stronger effect on the components of the BR signalling pathway than on the components of the GA signalling pathway. Our results also suggest that the interaction between transcription factors exerts more influence on the dynamics of the signalling pathways than BR signalling-mediated GA biosynthesis. Further, our results suggest that perturbations in the GA signalling pathway have larger effects on the dynamics of components of the BR signalling pathway than the perturbations in the BR signalling pathway on the dynamics of components of the GA signalling pathway, apart from in the case when we have disturbances in both the BR signalling pathway and the crosstalk mechanism.

The structure of this paper is as follows. In Section 2 a biological overview of the BR and GA signalling pathways, and their interactions is given. In Section 3 we derive the mathematical model for the BR signalling pathway and estimate the values for the model parameters using experimental data from [50]. In Section 4 we perform qualitative analysis of the model for the BR signalling pathway, examining how the behaviour of solutions of the mathematical model depends on the values of the model parameters. We also define the set of parameters for which the system of ODEs has stable stationary solutions and the set of parameters for which it undergoes Hopf bifurcation. In Section 5 we extend our model for the BR signalling pathway to examine the effects of spatial heterogeneity in the signalling processes. In Section 6 we consider the reduction of the mathematical model for the GA signalling pathway, proposed in [36], derive a new model for the crosstalk between BR and GA signalling pathways, and analyse the influence of different interaction mechanisms and changes in the dynamics of one of the signalling pathways on the qualitative and quantitative behaviours of the coupled system. We also analyse the influence of spatial heterogeneity of the signalling processes on the interactions between the BR and GA signalling pathways. We summarise and discuss our results in Section 7.

2 Biological Background

The mathematical modelling and analysis of the BR signalling pathway and of the interactions between the BR and GA signalling pathways is the main aim of this paper. In this section we present an overview of the BR and GA signalling pathways, and the interactions between them.

2.1 The BR Signalling Pathway

The signalling process starts at the cell plasma-membrane with the perception of BR by the receptor BRASSINOSTEROID INSENSITIVE1 (BRI1) [29]. Upon BR binding to BRI1, two main

events then take place, association of BRI1 to a co-receptor, BRI1-ASSOCIATED RECEPTOR KINASE1 (BAK1), and dissociation of the inhibitor protein BRI1 KINASE INHIBITOR1 (BKI1). This triggers a transphosphorylation cascade between BRI1 and BAK1, leading further to phosphorylation of BRASSINOSTEROID-SIGNALLING KINASE1 (BSK1), another membrane-bound kinase. Next, BSK1 phosphorylates the protein phosphatase BRI1-SUPPRESSOR1 (BSU1), which dephosphorylates a protein kinase BRASSINOSTEROID INSENSITIVE2 (BIN2), eventually leading to its degradation [41]. In the absence of BR, phosphorylated BIN2 has a role in phosphorylating the two transcription factors, BRASSINAZOLE RESISTANT1 (BZR1) and BRI1-EMS-SUPPRESSOR1 (BES1) [30], also known as BZR2 (for the purposes of this paper it is unnecessary to distinguish between the two, so we refer to them jointly as BZR). When phosphorylated, BZR is less stable and thus more unlikely to activate or repress any of the 1000s of genes associated with BR signalling [42], it is also thought that association of phosphorylated BZR to a 14-3-3 protein inhibits its entry to the nucleus. PROTEIN PHOSPHOTASE 2A (PP2A) is responsible for the de-phosphorylation of BZR, which allows its entry into the nucleus and then its activation of BR responsive genes.

BZR functions as a repressor of certain genes associated with the biosynthesis of BR, notably for example CONSTITUTIVE PHOTOMORPHOGENESIS AND DWARFISM (CPD), DWARF4 (DWF4), ROTUNDIFOLIA3 (ROT3) and BRASSINOSTEROID-6-OXIDASE 1 (BR6ox1) [50]. That is, active, de-phosphorylated BZR inhibits production of BR. So, high levels of BR cause low levels of phosphorylated BZR, leading to inhibition of BR biosynthesis and decreasing levels of BR. Conversely, low levels of BR lead to high levels of phosphorylated BZR and activation of BR biosynthesis, increasing the levels of BR. This completes the negative feedback loop of the BR signalling pathway.

2.2 The GA Signalling Pathway

Gibberellin Signalling is achieved by enhancing the degradation of DELLA proteins, which influence the expression of GA-responsive genes [1]. GA molecules are perceived by the GA receptor, GIBBERELLIN INSENSITIVE DWARF1 (GID1), a nuclear-localised protein [55]. Analysis of GID1's structure revealed that it has a GA-binding pocket, with a flexible extension adjacent [45]. When GA binds to GID1, this extension undergoes conformational change, and covers the GA-binding pocket. When closed, the upper surface of this lid binds to DELLA proteins to form the GA.GID1.DELLA complex. The formation of the GA.GID1.DELLA complex enhances the degradation of DELLA proteins by mediating proteasome-dependent destabilization of DELLA proteins.

The GA signalling pathway exhibits negative feedback due to the influence of DELLAs on the expression of several genes which code components of the signalling pathway [65]. First, DELLA activates the GID1-encoding gene, leading to an increase in the translation of the GID1 protein. This means that in the absence of DELLAs, GID1 concentration also decreases which will slow down the proteasome-induced DELLA degradation, and that an abundance of DELLA leads to the production of more GID1 and enhances the DELLA degradation. Next, DELLA activates the transcription of genes encoding the enzymes GA 20-oxidase (GA20ox) and GA 3-oxidase (GA3ox). These enzymes catalyse several reaction steps in the GA biosynthesis pathway, meaning an abundance of DELLA increases both GA and GID1, leading to degradation of DELLA. Lastly, DELLA represses its own gene transcription.

2.3 Crosstalk between the BR and GA Signalling Pathways

The interaction of BRs and GAs has been receiving much attention, due to their shared nature as critical plant growth regulators, combined with the fact that they share many overlapping functions such as regulation of cell elongation [10, 54] and plant responses to abiotic stress [3, 16]. However despite the interest, the exact mechanisms of these interactions have remained largely unclear, save from the fact that they control expression of several genes [9]. There has been much evidence that the signalling processes of BR and GA converge at the level of BZR and DELLA interaction. Direct crosstalk in this fashion was shown in [32], where it was shown that overexpression of DELLA proteins

reduced both the abundance and transcriptional activity of BZR. This was found to be due to the formation of a complex of DELLA and BZR, which removed BZR’s transcriptional ability. There is also evidence of BRs regulating the biosynthesis of GAs, the so called “GA Synthesis” model of BR-GA crosstalk. Two main proposals have been made for the existence of this type of interaction. The effects of BR mutants on GA synthesis were examined in [53], and it was concluded that BZR enhances GA synthesis by activating synthesis of the GA3ox enzyme. In contrast to this the findings in [56] describe a much larger role for BZR in regulating GA synthesis. They provide evidence for a model where BZR activates the synthesis of the GA20ox enzyme, in addition to the effects described in [53]. Thus BZR would influence the biosynthesis of GA in exactly the same manner as DELLAs for other interactions, however the significance of this mechanism of crosstalk is not yet established [40, 52, 57].

3 Derivation of a Mathematical Model for the BR Signalling Pathway

In this section we derive a mathematical model of the BR signalling pathway. In order to build a simple, yet sufficiently accurate and efficient model incorporating BR biosynthesis negative feedback, we first construct a reduced reaction schematic that describes the pathway mechanism. This reduction is achieved via a simplification of two principal parts of the signalling pathway: the complex BR biosynthesis network, and the cytoplasm localized phosphorylation cascade. Hence, we build a model focussing on three key components, hormone (BR), inhibitor (BKI1) and transcription factor (BZR), Fig. 1.

In the mathematical model we consider the binding of free BR molecules to the BRI1 receptors leading to the dissociation of BKI1. This is modelled as an almost instantaneous reaction, with $BR + BRI1.BKI1$ interacting and resulting into $BR.BRI1 + BKI1$. In order to model the effects of the signalling cascade induced by the membrane-bound receptors and subsequent effects on the phosphorylation state of BZR, we assume that the effects of active receptors in triggering the cascade may be approximated by the free BKI1 that is released upon this activation. We further assume that the free BKI1 catalyses dephosphorylation of BZR-p and destabilises the BIN2 proteins, thus reducing the phosphorylation of BZR.

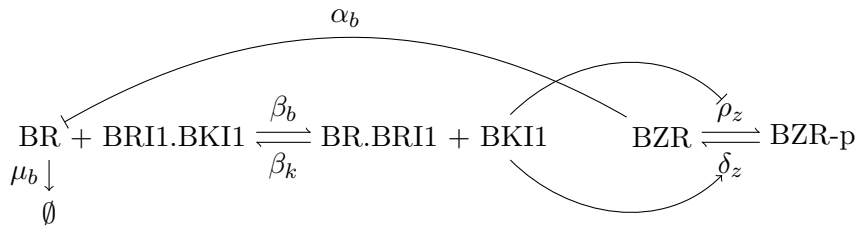


Figure 1: Reaction schematic of the reduced BR signalling pathway.

We denote by b the concentration of hormone BR, by k the concentration of inhibitor BKI1, by r_k the concentration of receptor-inhibitor complex BRI1.BKI1, by r_b the concentration of receptor-hormone complex BR.BRI1, by z the concentration of (dephosphorylated) transcription factor BZR, and by z_p the concentration of (phosphorylated) transcription factor BZR-p. Then assuming spatial homogeneity of the signalling processes, the interactions between b , k , r_k , r_b , z , and z_p are described by the system

of six ordinary differential equations

$$\begin{aligned}
\frac{db}{dt} &= \beta_k r_b k - \beta_b r_k b + \frac{\alpha_b}{1 + (\theta_b z)^{h_b}} - \mu_b b, \\
\frac{dk}{dt} &= \beta_b r_k b - \beta_k r_b k, \\
\frac{dr_k}{dt} &= \beta_k r_b k - \beta_b r_k b, \\
\frac{dr_b}{dt} &= \beta_b r_k b - \beta_k r_b k, \\
\frac{dz}{dt} &= \delta_z z_p k - \rho_z \frac{z}{1 + (\theta_z k)^{h_z}}, \\
\frac{dz_p}{dt} &= -\delta_z z_p k + \rho_z \frac{z}{1 + (\theta_z k)^{h_z}}.
\end{aligned} \tag{1}$$

Here β_b is the binding rate of b to r_k , and β_k is the binding rate of k to r_b . We model this as only two reactions by assuming that when either BR or BKI1 are bound to BRI1 either dissociates sufficiently fast that the levels of the BR.BRI1.BKI1 remains roughly zero. We assume the reaction to occur in some finite closed volume, so the loss of BR is only described by the degradation coefficient μ_b .

The phosphorylation state of BZR is modelled as being dependent on the levels of free BKI1. We justify this by noting that upon signalling activation, the receptor phosphorylates BSU1 which governs the phosphorylation of BZR via BIN2. Thus since BKI1 is also released upon BR binding, we may model these effects by assuming that free BKI1 activates (or catalyses) the dephosphorylation of BZR-p at rate δ_z . In BKI1's absence BZR is phosphorylated at rate ρ_z , and when BKI1 is present it inhibits the phosphorylation of BZR such that when $k = 1/\theta_z$, the rate of phosphorylation is halved.

Finally we model BR biosynthesis as being directly inhibited by BZR. BZR represses the expression of several genes encoding enzymes, namely CPD, DWF4, ROT3 and BR6ox1, that are required for the conversion of many of the precursors involved in BR biosynthesis. Hence we use a Hill function with exponent $h_b > 1$ to model the cumulative inhibitory effect of BZR on these genes. We estimate the parameter h_b by considering the detailed BR biosynthesis pathway(s) presented in [11]. The BR-mediated enzymes that are involved in the biosynthesis are CPD, DWF4, ROT3, and BR6ox1 which mediate four, five, six, and five steps in the biosynthetic pathway respectively. Since BR biosynthetic enzymes act multiplicatively at different steps of the reaction network, the expressions modelling their actions can be approximated by the product of these expressions, which would mean that the exponents of these functions would be summed, thus we consider $h_b = 20$.

The model equations (1) imply that the total concentrations of BKI1, BRI1 and BZR are conserved, thus we consider $k + r_k = K_{tot}$, $r_b + r_k = R_{tot}$, and $z + z_p = Z_{tot}$, and derive a reduced model:

$$\begin{aligned}
\frac{db}{dt} &= \beta_k (R_{tot} - K_{tot} + k)k - \beta_b (K_{tot} - k)b + \frac{\alpha_b}{1 + (\theta_b z)^{h_b}} - \mu_b b, \\
\frac{dk}{dt} &= \beta_b (K_{tot} - k)b - \beta_k (R_{tot} - K_{tot} + k)k, \\
\frac{dz}{dt} &= \delta_z (Z_{tot} - z)k - \rho_z \frac{z}{1 + (\theta_z k)^{h_z}}.
\end{aligned} \tag{2}$$

Various values for R_{tot} were reported in [59], and we chose the value for WT seedling roots. We further assume that $K_{tot} = R_{tot}$ in order that the receptor should have the ability to be completely inactive, but not be saturated by BKI1. We also use physiological values reported in the literature in order to write β_k and μ_b in terms of other parameters, for full calculations see A. As such we are left with 8 parameters for which we have no direct estimate, namely β_b , α_b , θ_b , δ_z , Z_{tot} , ρ_z , θ_z and h_z . These parameters were estimated indirectly by validating the numerical solutions of the mathematical model (2) against experimental results, using numerical optimisation algorithms.

By deriving the steady state concentration of BR, denoted $[BR]_0$, from the level of endogenous 24-epiBL reported in [62], we were able to write the rate of BR degradation μ_b in terms of α_b , θ_b , Z_{tot} , δ_z , ρ_z , θ_z , h_z and h_b as follows

$$\mu_b = \frac{\alpha_b}{[BR]_0 \left(1 + \left(\theta_b \frac{Z_{tot}\delta_z[BKI1]_0(1+(\theta_z[BKI1]_0)^{h_z})}{\rho_z + \delta_z[BKI1]_0(1+(\theta_z[BKI1]_0)^{h_z})} \right)^{h_b} \right)}. \quad (3)$$

We can write β_k in terms of β_b and other known parameters in two ways. First, using $[BR]_0$ in conjunction with the dissociation constant of BR.BRI1, denoted K_d , reported in [64] we can estimate the steady state concentration of BKI1, denoted $[BKI1]_0$, and write β_k in terms of $[BR]_0$, $[BKI1]_0$, K_{tot} , R_{tot} , and β_b as follows

$$\beta_k = \frac{(K_{tot} - [BKI1]_0)[BR]_0}{(R_{tot} - K_{tot} + [BKI1]_0)[BKI1]_0} \beta_b, \quad (4)$$

by assuming that the dissociation constant for BR.BRI1 depends on the steady state concentrations of BR, BR.BKI1 and BR.BRI1. For the second expression we considered the dissociation of both BR and BKI1 from BR.BRI1.BKI1, using the value for the dissociation constant of BKI1, denoted K_m , reported in [61], as well as K_d , to directly write β_k in terms of β_b as

$$\beta_k = \frac{K_d}{K_m} \beta_b. \quad (5)$$

These two constraints (4) and (5) on β_k correspond to two different mechanisms for the interactions between BR, BRI1 and BKI1. In (4) binding of BR to BRI1.BKI1 causes instantaneous dissociation of BKI1 and formation of BR.BRI1, likewise binding of BKI1 to BR.BRI1 causes instantaneous dissociation of BR and formation of BRI1.BKI1. In (5) binding of BR to BRI1.BKI1 or binding of BKI1 to BR.BRI1 leads to the formation of BR.BRI1.BKI1, which may then dissociate into either BKI1 and BR.BRI1, or BR and BRI1.BKI1. Model (2) was fitted to experimental data using both conditions (4) and (5) in order to compare their effects, see Figs. 2 and 3.

The experimental data from [50], used to determine model parameters, give the relative BR biosynthetic gene expression of CPD, DWF4, ROT3, and BR6ox1, and were measured by RT-PCR analysis, then converted to give relative values with the initial values equal to one. Values were measured for three independent experiments (three replicates), and the data presented by points and (where available) error bars correspond to the mean and standard error respectively. Gene expression was measured in both Wild-Type (WT) and *bri1-401* mutant (where perception of BR by BRI1 is inhibited) plants, and this was accounted for in our parameter estimation by assuming that the parameter β_b was greater for the WT than for the mutant. β_k was allowed to vary freely for the mutant case since constraints (4) and (5) are not definitely valid in this case. Both of these phenotypes were grown under control conditions as well as two other cases: one where plants were grown in a medium containing 5 μM of Brassinazole (BRZ), a BR-specific biosynthesis inhibitor, and one grown in a medium containing 0.1 μM of Brassinolide (BL) having first been grown in the medium containing 5 μM BRZ for two days. Data comparing the control case with the case of growth in the 5 μM BRZ medium were recorded for five days. Data comparing further growth after two days of the BRZ medium case with the case of addition of 0.1 μM BL to the medium were recorded for further 24 h, and as such for these cases the initial conditions were taken to be the values of the numerical solution to the model for the 5 μM BRZ medium at time $t = 2$ days. For the control conditions we made no amendments to the model, for the case of plants growing in the BRZ-medium we imposed bounds upon the parameters such that α_b should be smaller in this case since addition of BRZ reduces the biosynthesis of BR. In order to examine the case where BL was added to the growth medium, an extra term governing influx of exogenous BL and efflux of endogenous BR was added to the equation describing BR dynamics

$$\frac{db}{dt} = \beta_k(R_{tot} - K_{tot} + k)k - \beta_b(K_{tot} - k)b + \frac{\alpha_b}{1 + (\theta_b z)^{h_b}} - \mu_b b + \phi_b(\omega_b - b),$$

where ϕ_b is the relative permeability of the cell membrane to BR and was one of the optimised parameters for the relevant cases, and ω_b is assumed to be $0.1 \mu\text{M}$ in accordance with the experimental procedure.

Optimisation was achieved by comparing the biosynthetic expression defined by the numerical solutions of model (2), the term $1/(1 + (\theta_b z)^{h_b})$, with experimental data presented in [50]. In order to compare experimental data with the output from our model we first normalised the simulation data by their initial values such that they took values comparable to the experimental data. We then took the mean of the four gene data sets, weighted by the number of times the respective proteins appear in the biosynthetic pathway. The optimisation was carried out in Python using the `curve_fit` function in the `SciPy` module [26]. `curve_fit` applies nonlinear least squares minimization using the trust region reflective algorithm as default, with a default tolerance of 10^{-8} . The model was fitted to the data set for each case sequentially, starting with the WT under control conditions since this data set was the largest. The parameters μ_b and β_k were replaced by the expressions (3) and (4) or (5), respectively, for the WT data under control conditions since this is the only case where such parameter constraints are definitely valid. The parameters generated from the fitting for WT under control conditions were then used as the initial guesses for all other cases, where μ_b and β_k were also allowed to be fitted. Parameters that were not expected to vary under the different growth conditions were allowed very small variations to account for error in the first fitting, whereas parameters that were expected to vary had much wider bounds.

Numerical simulations of model (2) using the optimised parameters, given in Tables 1 and 2 for β_k determined by (4) and (5) respectively, are plotted against the experimental data in Fig. 2 and 3 and show good agreement with experimental data, having R^2 values of 0.89 and 0.92 respectively.

Constant	Value	Units	Source	Constant	Value	Units	Source
α_b	0.27	$\mu\text{M min}^{-1}$	fit	θ_z	3.95	μM^{-1}	fit
β_b	8.33	$\mu\text{M}^{-1} \text{min}^{-1}$	fit	h_b	20		[11]
β_k	2.73	$\mu\text{M}^{-1} \text{min}^{-1}$	(4)	h_z	6		fit
ρ_z	1.33×10^{-4}	min^{-1}	fit	K_{tot}	6.2×10^{-2}	μM	fit
δ_z	1.02×10^{-3}	$\mu\text{M}^{-1} \text{min}^{-1}$	fit	R_{tot}	6.2×10^{-2}	μM	[59]
μ_b	3.58	min^{-1}	(3)	Z_{tot}	2.65	μM	fit
θ_b	1.96	μM^{-1}	fit	ϕ_b	7.06	min^{-1}	fit
ω_b	0.1	μM	[50]				

Table 1: The model parameters associated with the BR signalling pathway model (2) for WT when fitted using expression (4) for β_k , together with their sources (Parameter set 1).

4 Qualitative Analysis of the Mathematical Model for the BR Signalling Pathway

In this section we consider well-posedness and qualitative analysis of model (2). We start by non-dimensionalising our model, transforming the variables as $t = \frac{1}{\mu_b} \bar{t}$, $b = \frac{\alpha_b}{\mu_b} \bar{b}$, $k = K_{tot} \bar{k}$, $z = Z_{tot} \bar{z}$, and introducing the dimensionless parameters

$$\bar{\beta}_k = \frac{\beta_k K_{tot}^2}{\alpha_b}, \quad \bar{\beta}_b = \frac{\beta_b K_{tot}}{\mu_b}, \quad \kappa = \frac{R_{tot}}{K_{tot}}, \quad \bar{\theta}_b = \theta_b Z_{tot},$$

$$\epsilon = \frac{\alpha_b}{K_{tot} \mu_b}, \quad \bar{\delta}_z = \frac{\delta_z K_{tot}}{\mu_b}, \quad \bar{\rho}_z = \frac{\rho_z}{\mu_b}, \quad \bar{\theta}_z = \theta_z K_{tot},$$

Constant	Value	Units	Source	Constant	Value	Units	Source
α_b	0.27	$\mu\text{M min}^{-1}$	fit	θ_z	3.95	μM^{-1}	fit
β_b	8.33	$\mu\text{M}^{-1} \text{min}^{-1}$	fit	h_b	20		[11]
β_k	2.18×10^{-2}	$\mu\text{M}^{-1} \text{min}^{-1}$	(5)	h_z	6		fit
ρ_z	4.26×10^{-4}	min^{-1}	fit	K_{tot}	6.2×10^{-2}	μM	fit
δ_z	1.75×10^{-3}	$\mu\text{M}^{-1} \text{min}^{-1}$	fit	R_{tot}	6.2×10^{-2}	μM	[59]
μ_b	3.68	min^{-1}	(3)	Z_{tot}	2.68	μM	fit
θ_b	2.0	μM^{-1}	fit	ϕ_b	160.93	min^{-1}	fit
ω_b	0.1	μM	[50]				

Table 2: The model parameters associated with the BR signalling pathway model (2) for WT when fitted using expression (5) for β_k , together with their sources (Parameter set 2).

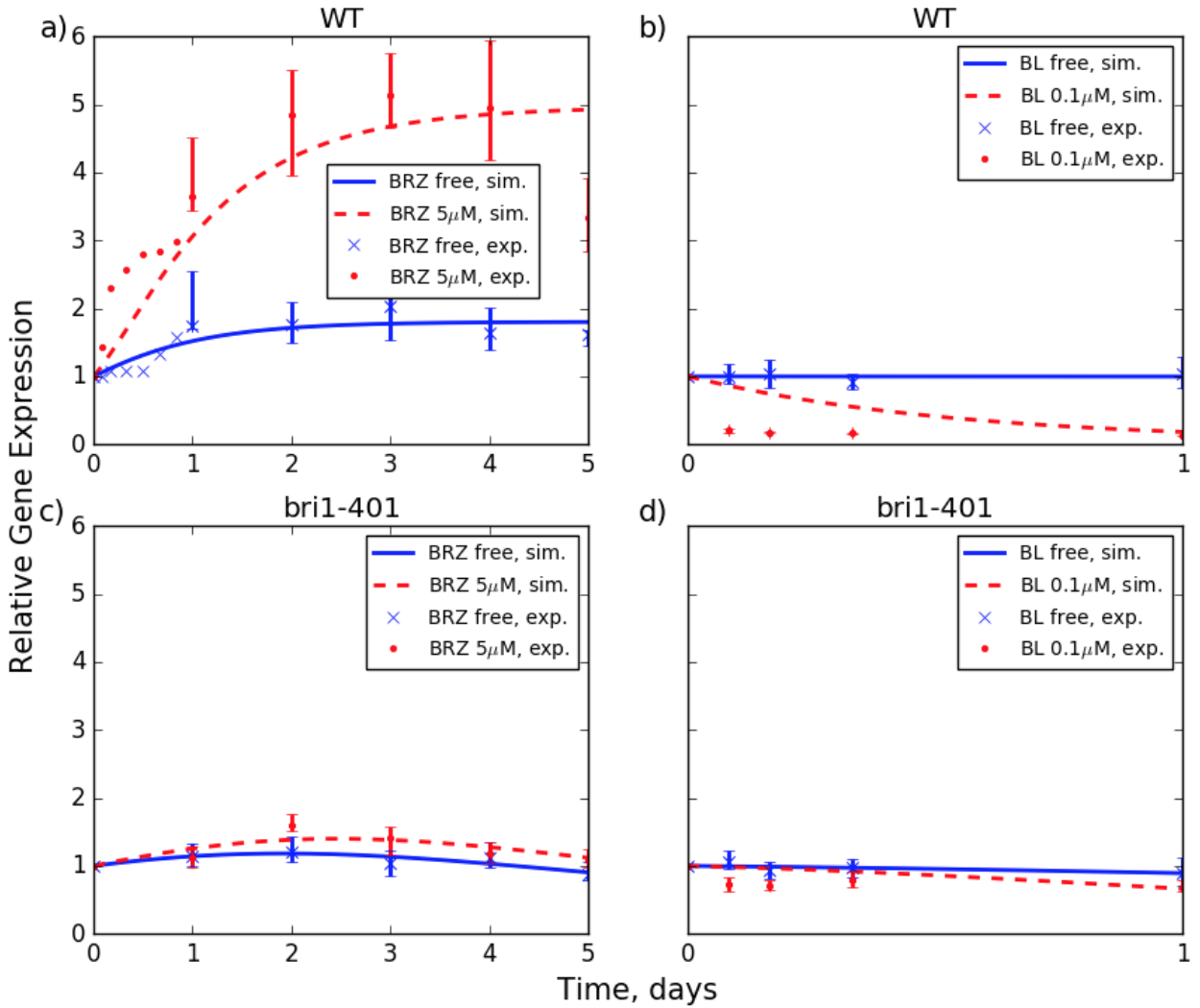


Figure 2: BR biosynthetic gene expression calculated from the numerical solutions of model (2), plotted against experimental data from [50]. For the WT plants grown under control conditions the parameters given in Table 1 were used, parameter sets for other cases can be found in Table 6.

which yields the system (neglecting \overline{s})

$$\begin{aligned}
 \frac{db}{dt} &= f_1(b, k, z) = \beta_k(\kappa - 1 + k)k - \beta_b(1 - k)b + \frac{1}{1 + (\theta_b z)^{h_b}} - b, \\
 \frac{dk}{dt} &= f_2(b, k, z) = \frac{1}{\epsilon} (\beta_b(1 - k)b - \beta_k(\kappa - 1 + k)k), \\
 \frac{dz}{dt} &= f_3(b, k, z) = \delta_z(1 - z)k - \rho_z \frac{z}{1 + (\theta_z k)^{h_z}}.
 \end{aligned} \tag{6}$$

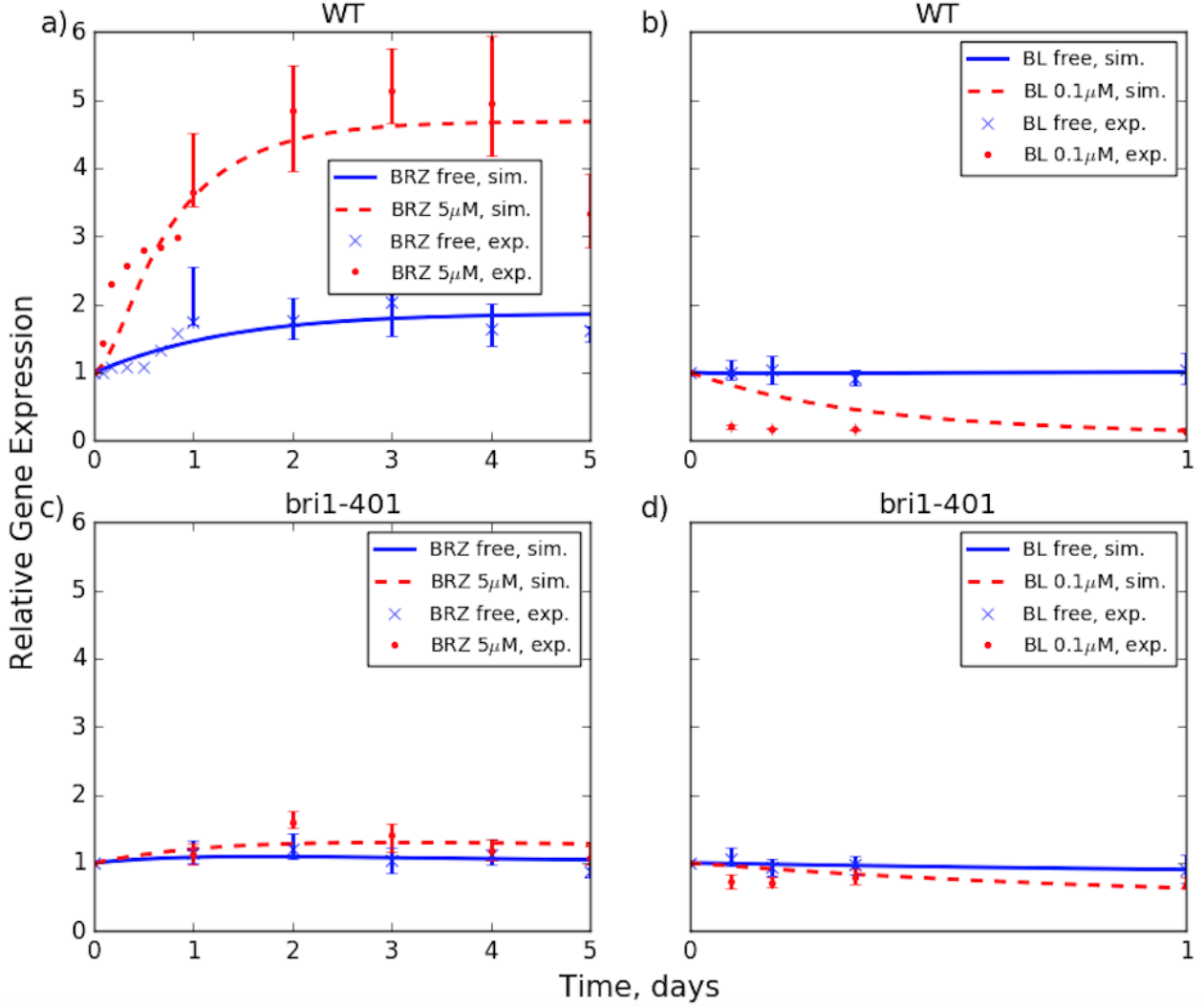


Figure 3: BR biosynthetic gene expression calculated from the numerical solutions of model (2), plotted against experimental data from [50]. For the WT plants grown under control conditions the parameters given in Table 2 were used.

For simplicity of presentation we denote by $P \subset [1, \infty) \times \mathbb{R}_+^7 \times \mathbb{N}^2$ the parameter space for system (6), where for each $p \in P$, $p = (\kappa, \beta_k, \beta_b, \theta_b, \epsilon, \delta_z, \rho_z, \theta_z, h_b, h_z)$. We assume that κ has a minimum value of 1 since $\kappa < 1$ would imply saturation of receptor by inhibitor (i.e. $K_{tot} > R_{tot}$), leading to BR signalling being permanently switched on.

Theorem 1. *The system (6) has a unique, global solution $(b, k, z) \in C^1([0, \infty))$ for any initial value $(b^0, k^0, z^0) \in [0, 1 + \beta_k \kappa] \times [0, 1]^2$, and $(b(t), k(t), z(t)) \in [0, 1 + \beta_k \kappa] \times [0, 1]^2$ for all $t \in [0, \infty)$ and any $p \in P$.*

Proof. Define $u = (b, k, z)^T$ and $\mathbf{f} = (f_1, f_2, f_3)^T$, and hence $\frac{du}{dt} = \mathbf{f}$. Since \mathbf{f} is locally Lipschitz-continuous, the Picard-Lindelöf theorem ensures local existence of a unique solution of (6), see e.g. [5]. To obtain global existence and uniqueness we prove boundedness of solutions by demonstrating the existence of a positive-invariant region for system (6), i.e. showing that for a solution u of (6) starting in $M = [0, 1 + \beta_k \kappa] \times [0, 1] \times [0, 1]$ it will always be contained within this region. To show that a region M is positive invariant under the flow of system (6), we show that $\mathbf{f}(u) \cdot \mathbf{n}(u) \geq 0 \forall u \in \partial M$, see e.g. [5], where \mathbf{n} is the inward normal vector on ∂M , see B.1 for more details. This implies uniform boundedness of solutions of (6) with initial values in M , and continuous differentiability of f ensures global existence and uniqueness. \square

Theorem 2. *For any parameter set $p \in P$, there exists a unique steady state solution $(b^*, k^*, z^*) \in M$ of system (6).*

Proof. Considering equations for a steady state solution (b^*, k^*, z^*) of (6) and employing simple algebraic manipulation, k^* is defined as a root of the following non-linear function

$$g(k^*) := \beta_k (\kappa - 1 + k^*) k^* \left(1 + \left(\frac{\theta_b \delta_z k^* (1 + (\theta_z k^*)^{h_z})}{\rho_z + \delta_z k^* (1 + (\theta_z k^*)^{h_z})} \right)^{h_b} \right) - \beta_b (1 - k^*),$$

and b^* and z^* are determined as functions of k^* , for more details see B.2. We may immediately see, since $g(0) = -\beta_b$ and $g(1) = \beta_k \kappa (1 + (\theta_b \delta_z (1 + \theta_z^{h_z}) / (\rho_z + \delta_z (1 + \theta_z^{h_z})))^{h_b})$, that g must contain at least one root in $[0, 1]$ for any $p \in P$, and hence system (6) must contain at least one steady state solution in M . In order to find the number of roots of $g(k^*) = 0$ in $[0, 1]$, consider the derivative of g which is positive for all $p \in P$ and $k^* \in [0, 1]$, see B.2 for the formula for $g'(k^*)$. Thus g is monotonically increasing. Strict monotonicity of g coupled with existence of at least one root in $[0, 1]$ implies that g has a unique root in $[0, 1]$, and hence (6) has a unique steady state in M . \square

4.1 Linearised Stability and Bifurcation Analysis

To study the qualitative behaviour of solutions of mathematical model for BR signalling pathway, we performed linearised stability analysis for system (6) and analyse the impact of variations in values of model parameters on the behaviour of solutions of (6). For the parameters obtained via validation of mathematical model by experimental data, see Tables 1 and 2, steady state solutions of (6) are linearly stable, with eigenvalues $(-3.8764, -0.1508, -0.0009)$ and $(-3.6863, -0.1138, -0.0006)$ respectively. Further, stability of steady state solutions is maintained under moderate variations of all parameters, suggesting that the BR homeostasis is ensured in normally functioning plant cells. Large variations in δ_z , ρ_z , and θ_z however cause qualitative changes in the behaviour of solutions of model (2) and can induce oscillatory behaviour, but only in the case when all other parameters are as in Table 1 and not as in Table 2. We consider δ_z and ρ_z as bifurcation parameters because these parameters directly correspond to processes in the BR signalling pathway, whereas $1/(1 + (\theta_z k)^{h_z})$ is only an approximation for the dynamics of the cytoplasmic phosphorylation cascade. Biologically, increase of δ_z could potentially correspond to faster phosphorylation of BSU1 by BAK1, or decrease of δ_z corresponding to reduced action of PP2A in dephosphorylating BZR. Further, decrease of ρ_z could correspond to BIN2-deficient or insensitive mutants e.g. bes1-D, and increase of ρ_z could correspond to BIN2-overexpressing mutants, e.g. bin2. In the bifurcation analysis of system (2) we considered increased value for the dimensional parameter θ_z compared to the standard value, Table 1 (i.e. $\theta_z = 41.2 \mu\text{M}^{-1}$), which was essential to determine the region for parameters δ_z and ρ_z where system (6) undergoes bifurcation. For the value of $\theta_z = 3.95 \mu\text{M}^{-1}$ obtained through fitting model solutions to experimental data, the steady state solution of (6) is linearly stable for a wide range of values of δ_z and ρ_z , i.e. $\delta_z, \rho_z \in (0, 50)$.

Theorem 3. *As δ_z and ρ_z are continuously varied, system (6) undergoes a Hopf bifurcation.*

Proof. We performed linearised stability analysis to determine the parameter subspace for which the stationary solution of (6) is linearly stable, as well as the range of parameters for which we have periodic solutions for the model (6).

Using the Jacobian (28) of system (6), evaluated at the steady-state (b^*, k^*, z^*) , we calculate the characteristic equation for the system to be a cubic polynomial of the form $\lambda^3 + a_2 \lambda^2 + a_1 \lambda + a_0 = 0$, where a_2 , a_1 and a_0 are all positive, real constants (see B.3). Since the characteristic equation is a cubic polynomial we obtain that there are only 2 possible sets of eigenvalues, either that they are all real or that there is one real eigenvalue λ_1 and two complex conjugate eigenvalues λ_2 and λ_3 . Further, since all coefficients have the same sign any real eigenvalue must be negative, specifically zero cannot be an eigenvalue of J for any parameters of system (6) in P . Together these two facts tell us that in the case where the eigenvalues are all real, or that the complex conjugate eigenvalues have negative real part the steady state is stable, and that there is a possible bifurcation point when the two complex

conjugate eigenvalues cross the imaginary axis, corresponding to a Hopf bifurcation.

We showed numerically that for a closed loop \mathcal{L} in (δ_z, ρ_z) the system has complex conjugate eigenvalues with zero real parts, Fig. 4, and in the region \mathcal{D} enclosed by the loop \mathcal{L} the complex conjugate eigenvalues have positive real part, whereas for $(\delta_z, \rho_z) \in (0, 50)^2 \setminus \overline{\mathcal{D}}$ the real part of the complex conjugate eigenvalues is negative. Hence the points of the loop \mathcal{L} correspond to the bifurcation points where the stability of stationary solutions of (6) changes. We also showed that at such points the eigenvalues have non-zero imaginary parts and hence do not pass through the origin, Fig. 5a), which supports the proof of the fact that zero cannot be an eigenvalue of J , presented above. For this we designed a scheme in MATLAB to calculate the eigenvalues of the Jacobian J in (28), for values of $(\delta_z, \rho_z) \in (0, 50)^2$, with dimensional parameter values $\theta_z = 41.2 \mu\text{M}^{-1}$ and all other parameters as in Table 1. For each $\delta_z \in (0, 50)$, we determined the values of $\rho_z \in (0, 50)$ for which J has a pair of non-zero purely imaginary eigenvalues. The derivatives of the real part of the eigenvalues w.r.t. both δ_z and ρ_z were also calculated numerically, Fig. 5b). The values of $\frac{d}{d\delta_z} \text{Re}(\lambda_{2,3})$ and $\frac{d}{d\rho_z} \text{Re}(\lambda_{2,3})$ at the critical points are non-zero, apart from exactly four points on the curve in Fig 5b), where the derivative w.r.t. one of the parameters will be zero. Those four points correspond to the points where δ_z or ρ_z are at their extreme values, i.e. when δ_z takes an extreme value we have that $\frac{d}{d\rho_z} \text{Re}(\lambda_{2,3}) = 0$, and when ρ_z takes an extreme value that $\frac{d}{d\delta_z} \text{Re}(\lambda_{2,3}) = 0$. When δ_z is fixed at an extreme point, varying ρ_z will not cause the point to enter the region bounded by the curve and will not correspond to a bifurcation point w.r.t. ρ_z , similar for ρ_z fixed at an extreme point. Hence zero derivative at this point does not break the transversality condition. Thus, in conjunction with Theorems 1 and 2 we have shown that system (6) satisfies all conditions for the existence of a local Hopf bifurcation [24].

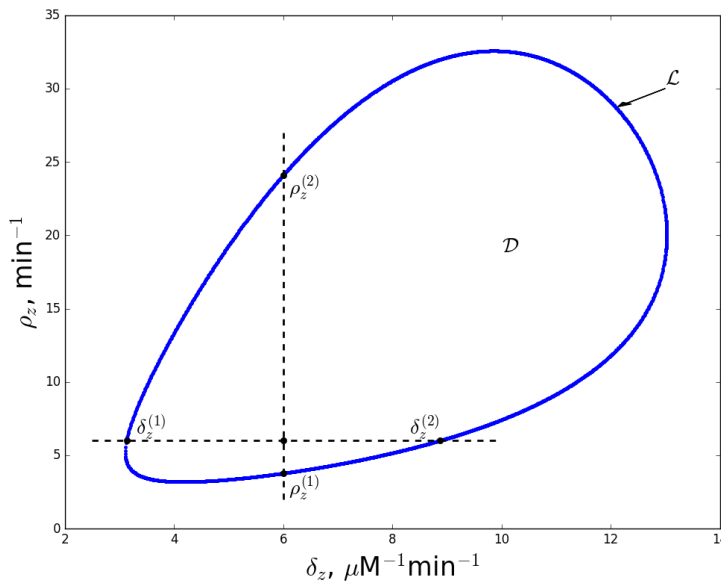


Figure 4: Critical dimensional values δ_z and ρ_z , at which the complex conjugate pair of eigenvalues λ_2, λ_3 of (28) are purely imaginary, form a closed curve \mathcal{L} . Note the third eigenvalue λ_1 is always negative. The system (6) exhibits oscillatory behaviour when values of (δ_z, ρ_z) are located within the region \mathcal{D} bounded by curve. For $\delta_z = 6$ fixed, the eigenvalues cross the imaginary axis at $\rho_z^{(1)} = 3.78$ and $\rho_z^{(2)} = 24.1$ with values of $\frac{d}{d\rho_z} \text{Re}(\lambda_{2,3})$ of 1.78×10^{-3} and -4.53×10^{-4} respectively. For $\rho_z = 6$ fixed, the eigenvalues cross the imaginary axis at $\delta_z^{(1)} = 3.14$ and $\delta_z^{(2)} = 8.87$ with values of $\frac{d}{d\delta_z} \text{Re}(\lambda_{2,3})$ of 2.73×10^{-3} and -1.33×10^{-3} respectively.

Therefore, for all parameter sets such that $(\delta_z, \rho_z) \in (0, 50)^2 \setminus \overline{\mathcal{D}}$, $\theta_z = 41.2 \mu\text{M}^{-1}$, and all other dimensional parameters are defined as in Table 1, we have that the steady state solution of system (6) is linearly stable. At the points $(\delta_z, \rho_z) \in \mathcal{L}$ the system (6) undergoes a Hopf bifurcation, and for $(\delta_z, \rho_z) \in \mathcal{D}$ we have periodic solutions for the BR signalling pathway model. \square

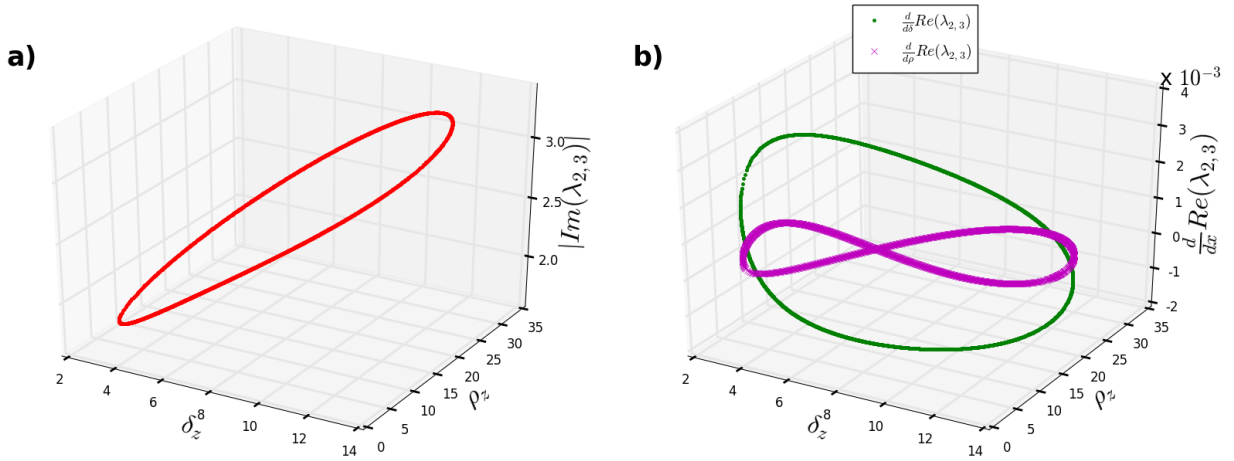


Figure 5: Numerical verification of the existence of a Hopf bifurcation. **a)** at the critical values, $Im(\lambda_{2,3})$ are non-zero. **b)** derivatives of $Re(\lambda_{2,3})$ w.r.t. both δ_z and ρ_z (green dots and magenta crosses respectively). Values pass through zero at the points of the curve in a) where δ_z or ρ_z take their extrema. At such points there is a bifurcation only in one of the parameters, the parameter for which $Re(\lambda_{2,3})$ has non-zero derivative.

5 Spatially Heterogeneous Model for the BR Signalling Pathway

The BR signalling pathway is a process which has distinct functions at different spatial locations in the cell, Fig. 6. Thus it is important to extend the ODE model (1) and analyse the dependence of the dynamics of the pathway components on the spatial distribution.

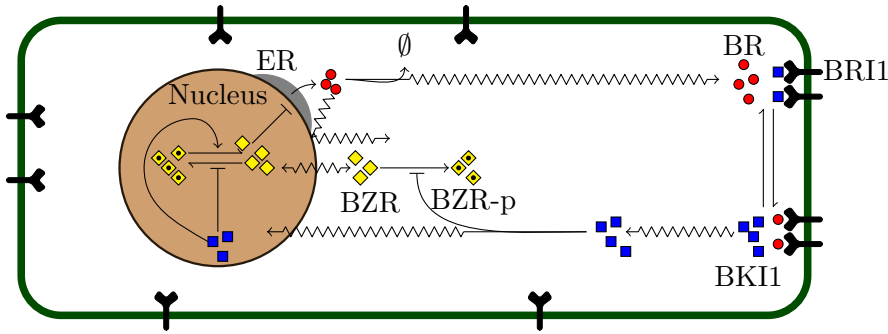


Figure 6: Diagram of the spatial heterogeneity considered for the model of the BR signalling pathway (7)-(9). BR (red circles), BKI1 (blue squares) and BZR-p (yellow diamonds with black dots) diffuse freely in the cytoplasm, where BR is also degraded. At the membrane, both BR and BKI1 are perceived by BRI1 (black y-shapes) and form complexes with it. In the nucleus (brown) BKI1 activates dephosphorylation of BZR-p to BZR (yellow diamonds), and inhibits phosphorylation of BZR to BZR-p. BR is synthesised in the endoplasmic reticulum (ER, grey crescent) which is continuous with the nuclear membrane.

We consider a spatially heterogeneous model for the BR signalling pathway in the one-dimensional domain $\Omega_c = (0, l_c)$ representing a part of the plant cell cytoplasm, where l_c denotes the length of the cell segment we consider. The boundaries of Ω_c are denoted by Γ_n modelling the cell nucleus, and Γ_c representing the cell membrane, Fig. 7.

We assume the diffusion of BR (b), BKI1 (k) and BZR-p (z_p) in the cytoplasm:

$$\left. \begin{aligned} \partial_t b &= D_b \partial_x^2 b - \mu_b b \\ \partial_t k &= D_k \partial_x^2 k \\ \partial_t z_p &= D_z \partial_x^2 z_p \end{aligned} \right\} \text{ in } \Omega_c. \quad (7)$$

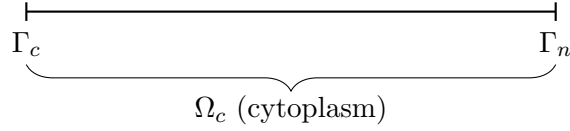


Figure 7: A diagram of the one-dimensional domain in which system (7)-(9) was solved. $\Omega_c = (0, l_c)$ represents the cytoplasm, Γ_c the plasma membrane, and Γ_n the nucleus.

The only reaction that takes place in Ω_c is the degradation of BR since we assume that the phosphorylation status of BZR is modulated only in the nucleus. The dynamics occurring on the plasma membrane Γ_c are the interactions between b , k , and receptor BRI1 (r_k , r_b). Since we assume that the receptors are membrane-bound a system of ODEs, similar to the corresponding equations in system (1), is considered to model the dynamics of r_k and r_b . The effect of the interactions between b , k , r_k , and r_b on the dynamics of b and k is defined by Robin boundary conditions for b and k on Γ_c . Finally, we assume that the BZR-p cannot diffuse out of the cell, which we model by a zero-flux boundary condition on Γ_c . Thus on Γ_c we have

$$\left. \begin{aligned} -D_b \partial_x b &= \beta_k \tilde{r}_b k - \beta_b \tilde{r}_k b \\ -D_k \partial_x k &= \beta_b \tilde{r}_k b - \beta_k \tilde{r}_b k \\ -D_z \partial_x z_p &= 0 \\ \frac{d\tilde{r}_k}{dt} &= \beta_k \tilde{r}_b k - \beta_b \tilde{r}_k b \\ \frac{d\tilde{r}_b}{dt} &= \beta_b \tilde{r}_k b - \beta_k \tilde{r}_b k \end{aligned} \right\} \text{ on } \Gamma_c. \quad (8)$$

In the nucleus Γ_n we consider both the phosphorylation and dephosphorylation of BZR. Although the exact subcellular location of BR biosynthesis has not been experimentally demonstrated, the likely location is the endoplasmic reticulum [46]. The endoplasmic reticulum is continuous with the nuclear membrane, hence we model the BR biosynthesis as occurring on Γ_n . We assume that BKI1 cannot enter the nucleus and consider zero-flux boundary conditions for k on Γ_n .

$$\left. \begin{aligned} D_b \partial_x b &= \frac{\tilde{\alpha}_b}{1 + (\tilde{\theta}_b \tilde{z})^{h_b}} \\ D_k \partial_x k &= 0 \\ D_z \partial_x z_p &= -\tilde{\delta}_z z_p k + \rho_z \frac{\tilde{z}}{1 + (\theta_z k)^{h_z}} \\ \frac{d\tilde{z}}{dt} &= \delta_z z_p k - \rho_z \frac{\tilde{z}}{1 + (\theta_z k)^{h_z}} \end{aligned} \right\} \text{ on } \Gamma_n. \quad (9)$$

Since \tilde{r}_k , \tilde{r}_b and \tilde{z} are confined to the boundary, they have units of mol/m^2 . Thus we have the following scaled relationships between variables \tilde{r}_k , \tilde{r}_b and \tilde{z} in (7)-(9) and the corresponding variables r_k , r_b and z in (1): $\tilde{r}_k = l_c r_k$, $\tilde{r}_b = l_c r_b$, $\tilde{z} = l_c z$. In order to preserve the balance of units some parameters from model (1) also had to be rescaled, specifically $\tilde{\alpha}_b = l_c \alpha_b$, $\tilde{\delta}_z = l_c \delta_z$ and $\tilde{\theta}_b = \theta_b / l_c$. We estimated the diffusion constant $D_b = 60 \mu m^2 min^{-1}$ by taking the value reported for Progesterone (a steroidal hormone with a similar structure to BL) in physiological solution from [47]. We also took $D_k = D_z = 0.125 \mu m^2 min^{-1}$ for the diffusion constant for proteins from [48]. l_c was taken to be $7.43 \mu m$ from measurements of root cell sizes from unpublished data. All other parameters were taken to be the same as in Table 1 or Table 2.

Model (7)-(9) was solved numerically to analyse the changes of the model solutions due to the spatial heterogeneity of signalling processes. In the fitted parameter regimes, averaged solutions of the model (7)-(9) have similar behaviour to solutions of (2), Fig. 8, however a distinct spatial distribution of BR is characteristic for (7)-(9), see Fig. 9. In the oscillatory parameter regime discussed in section 4.1, the PDE-ODE model (7)-(9) was found to have increased amplitude and period of oscillations, see Fig. 8. For solutions of model (7)-(9) we also observe oscillatory behaviour for a much wider range of values of δ_z and ρ_z than for model (2).

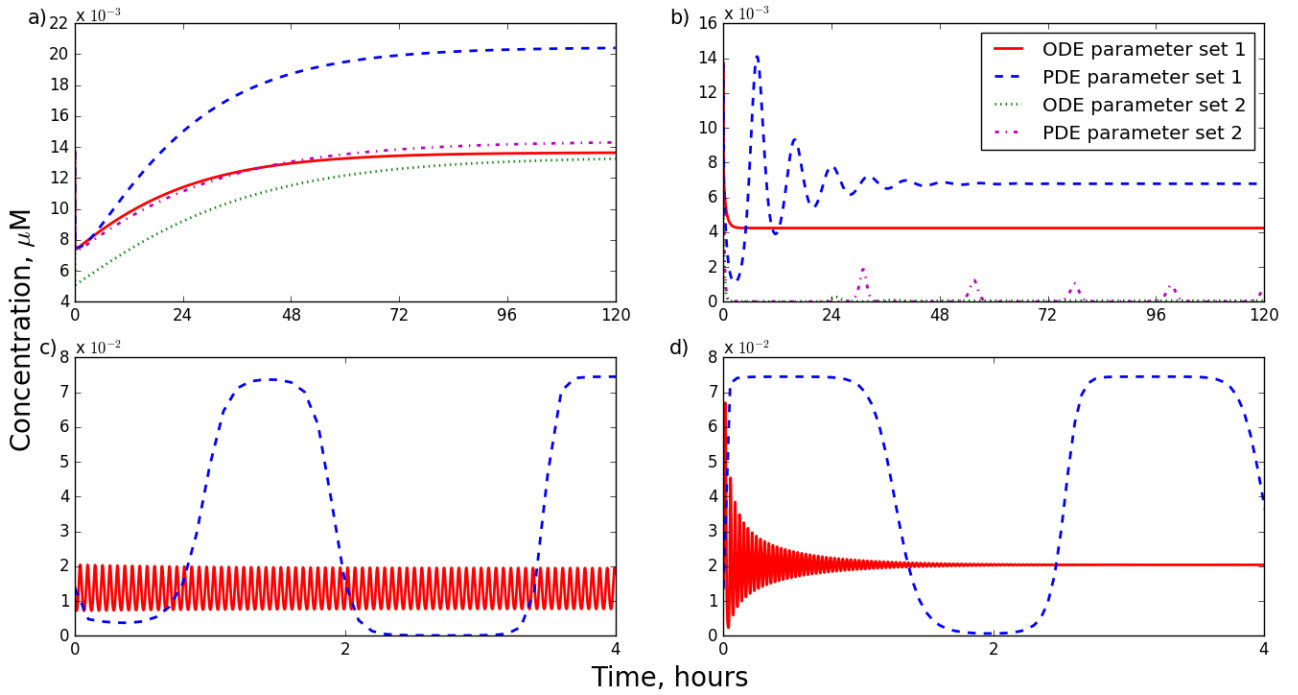


Figure 8: Comparison between the dynamics of BR for the ODE model (6), and the PDE-ODE model (7)-(9) for various parameter values. For comparison, the solutions to the PDE-ODE model have been averaged over the space, and the initial conditions are such that they are equal for the ODEs and the averaged PDEs. **a)** Both models were solved with the fitted parameters (parameters in Tables 1 and 2 correspond to set 1 and set 2 respectively), and show similar behaviour. **b)** Models were solved for $\delta_z = 1.02 \times 10^{-2}$, $\rho_z = 1.33 \times 10^{-3}$, $\theta_z = 41.2$ and all other parameters as in Tables 1 and 2 respectively. The ODE model tends quickly to steady state, whereas the PDE-ODE model exhibits damped oscillations. **c)** Models were solved for $\delta_z = \rho_z = 4$, $\theta_z = 41.2$, and all other parameters as in Table 1. Both systems exhibit periodic solutions, but the PDE-ODE model has a much reduced frequency and much increased amplitude as compared to the ODE model. **d)** $\delta_z = 14$, $\rho_z = 35$, $\theta_z = 41.2$, and all other parameters as in Table 1, ODE model has moved outside of the oscillatory parameter regime, however the same is not true for the PDE-ODE model, which continues to have oscillatory behaviour for values of δ_z , ρ_z in excess of 1000.

6 Derivation of a Mathematical Model for Crosstalk between the BR and GA Signalling Pathways

Here we consider a mathematical model for the crosstalk between the BR and GA signalling pathways. BRs and GAs can play similar independent roles in development both having important roles in growth [15, 54], as well as acting together via shared gene expression, and through interactions between their signalling pathways [9, 51]. We aim to use our model to analyse the three different mechanisms of crosstalk between the BR and GA signalling pathways proposed in [31, 53, 56] and to attempt to establish which mechanism has the most significant influence on the dynamics of the pathways.

6.1 Mathematical Modelling of GA Signalling

A detailed model of the GA signalling pathway was derived and examined in [36], consisting of a system of 21 ODEs and 42 parameters. It considers both the interaction of the GA_4 , $GID1$ and $DELTA$, and the GA_4 biosynthesis pathway, where GA_{12} is converted to GA_{15} is converted to GA_{24} is converted to GA_9 , all catalysed by enzyme GA_{20ox} , and GA_9 is converted to GA_4 , catalysed by GA_{3ox} .

Since a model for crosstalk must include variables for both pathways involved, as well as potentially introducing new variables specific to their interactions, a system of ODEs describing such a model

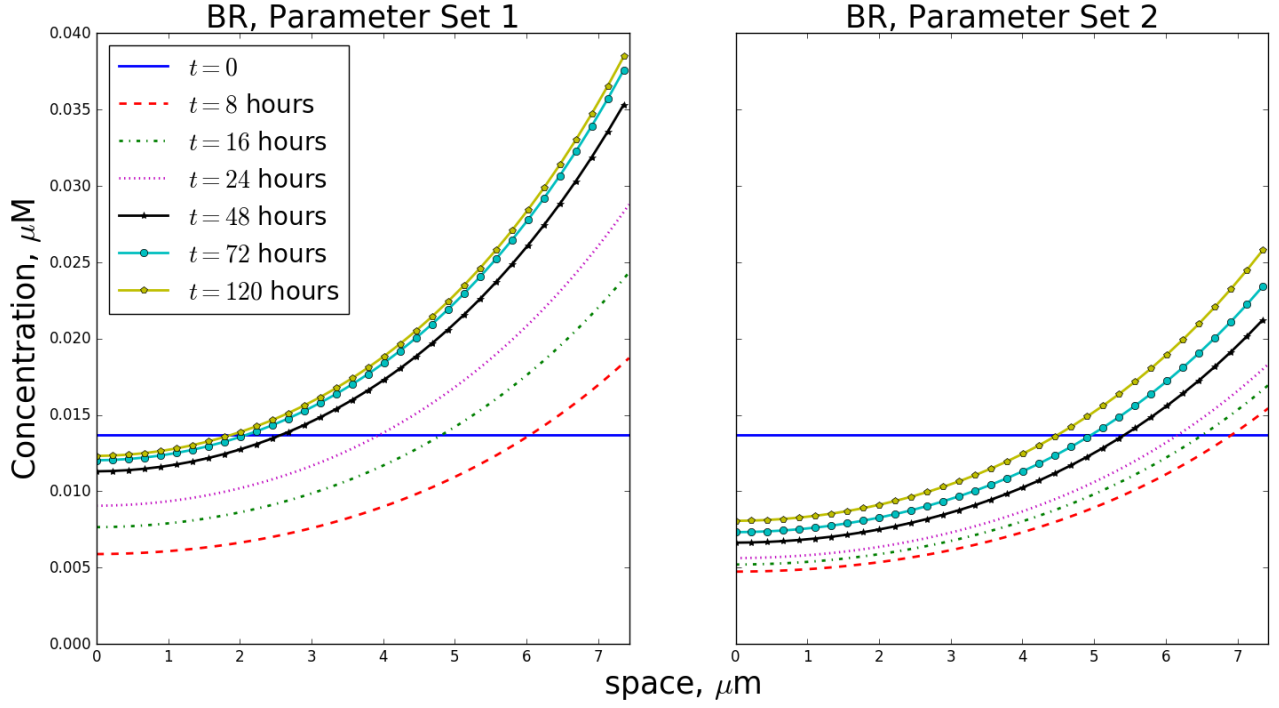


Figure 9: The spatial distribution of BR in the cell segment Ω_c , solution of (7)-(9), at different times, where ‘parameter set 1’ and ‘parameter set 2’ correspond to parameter values in Table 1 and Table 2 respectively. The steady state concentration of BR is greater for solutions with parameter set 1, Table 1, than for solutions with parameter set 2, Table 2.

may be very large. This being the case, we first reduce the size of the GA signalling model that was derived in [36]. We reduce the model by assuming that the dynamics of the molecules involved in the GA biosynthesis pathway are much faster compared to the dynamics of other processes involved in the signalling pathway that their levels remain at a steady state. This enables us to write a system of algebraic equations governing GA_{12} , GA_{15} , GA_{24} , GA_9 , GA_{20ox} and GA_{3ox} , as well as their relevant mRNAs and complexes which may then be solved such that they may therefore be substituted out of the main system. These substitutions generate a new term governing the biosynthesis of GA_4 , where biosynthesis is directly dependent on DELLA concentration, which is then simplified to a fourth order Hill function, signifying the 4 steps in the biosynthesis pathway. We also assume that only one configuration of $DELLA.GID1^c.GA_4$ may be formed. Overall this removes 27 parameters and 13 variables from the system in [36], and introduces a new term for the GA_4 biosynthesis with new parameters α_g and ϑ_g . The interested reader may examine both the reduction process as well as explicit calculations of α_g and ϑ_g in D. Then for r , r_g^o , r_g^c , r_d , r_m and d_m , the concentrations of GID1, $GID1^o.GA_4$, $GID1^c.GA_4$, $DELLA.GID1^c.GA_4$, GID1 mRNA and DELLA mRNA respectively, we obtain

$$\begin{aligned}
\frac{dr}{dt} &= -\beta_g r g + \gamma_g r_g^o + \alpha_r r_m - \mu_r r, \\
\frac{dr_g^o}{dt} &= \beta_g r g - \gamma_g r_g^o + \lambda^o r_g^c - \lambda^c r_g^o, \\
\frac{dr_g^c}{dt} &= -\lambda^o r_g^c + \lambda^c r_g^o - \beta_d d_l r_g^c + (\gamma_d + \mu_d) r_d, \\
\frac{dr_d}{dt} &= \beta_d d_l r_g^c - (\gamma_d + \mu_d) r_d, \\
\frac{dr_m}{dt} &= \phi_r \left(\frac{d_l}{d_l + \vartheta_r} - r_m \right), \\
\frac{dd_m}{dt} &= \phi_d \left(\frac{\vartheta_d}{d_l + \vartheta_d} - d_m \right),
\end{aligned} \tag{10}$$

and for d_l and g , the concentrations of DELLA and GA₄ respectively, we have

$$\begin{aligned} \frac{dd_l}{dt} &= -\beta_d d_l r_g^c + \gamma_d r_d + \alpha_d d_m, \\ \frac{dg}{dt} &= \phi_g(\omega_g - g) - \beta_g r g + \gamma_g r_g^o + \alpha_g \frac{d_l^4}{d_l^4 + \vartheta_g} - \mu_g g. \end{aligned} \quad (11)$$

Constant	Value	Units	Constant	Value	Units
β_g	1.35	$\mu\text{M}^{-1}\text{min}^{-1}$	γ_g	2.84	min^{-1}
α_r	19.3	$\mu\text{M min}^{-1}$	μ_r	3.51	min^{-1}
λ^o	0.0776	min^{-1}	λ^c	0.0251	min^{-1}
β_d	10	$\mu\text{M min}^{-1}$	γ_d	0.133	min^{-1}
μ_d	6.92	min^{-1}	α_d	5.28×10^{-4}	$\mu\text{M min}^{-1}$
ϕ_g	1.061×10^{-3}	min^{-1}	ω_g	154.27	μM
α_g	6.40×10^{-3}	$\mu\text{M min}^{-1}$	ϑ_g	4.27×10^{-13}	μM^4
μ_g	0.291	$\mu\text{M min}^{-1}$	ϕ_r	0.0457	min^{-1}
ϑ_r	5.6×10^{-4}	μM	ϕ_d	0.0708	min^{-1}
ϑ_d	0.01	μM			

Table 3: Default parameter values used for the GA signalling model. The values of all parameters except α_g and ϑ_g were taken directly from [36] from which our reduced model has been derived. The values for α_g and ϑ_g were calculated using the parameters from [36] and the expressions for α_g and ϑ_g arising from the model reduction, see D.

All parameter values are taken from those for the full model in [36], Table 3. For all components present in both the full and the reduced model, the initial conditions are taken to be the same as in [36]. Both the full and reduced models were solved numerically, and these solutions are plotted in Fig. 10. The two models show excellent agreement being almost indistinguishable for six terms, and only minor short-term discrepancies for DELLA.GID1^c.GA₄ and DELLA. Having thus successfully reduced the GA signalling pathway model while retaining its core behaviour, we derive a model of the crosstalk between the BR and GA signalling pathways by coupling models (2) and (10), (11).

6.2 The Crosstalk Model

We consider direct crosstalk between the BR and GA signalling pathways. Besides shared gene expression, two main mechanisms for BR-GA crosstalk have been suggested: direct interaction at the level of transcription factors BZR and DELLA [31], and BZR-mediated biosynthesis of GA [56]. Here we derive a mathematical model to compare the behaviour of the system under the three different mechanisms of crosstalk (interaction between BZR and DELLA, BZR-mediated biosynthesis of GA, and a combination of both of them) and to analyse their effects on the BR and GA signalling processes.

The existence of an interaction between BZR and DELLA constituting a crosstalk between the BR and GA signalling pathways was established in [6, 20, 32]. Further to this, in [31] it was found that the formation of a complex BZR.DELLA inhibits the transcriptional activities of both BZR and DELLA. A second mechanism of BR-GA crosstalk has been proposed where BZR also has a direct influence on the GA₄ biosynthesis pathway, Fig. 12. In [53] it was discovered that BR induces the expression of GA3ox-2, leading to the accumulation of GA₁, the most bioactive GA for rice. It was also discovered that the external application of BR induces GA20ox expression in Arabidopsis [33]. Later it was shown that BRs both regulate GA20ox expression, and are required for the transcription of GA3ox [56]. Despite good evidence for the coexistence of these two mechanisms, it is still unclear to what extent each mechanism operates to effect changes in BR and GA signalling processes [40, 52, 57].

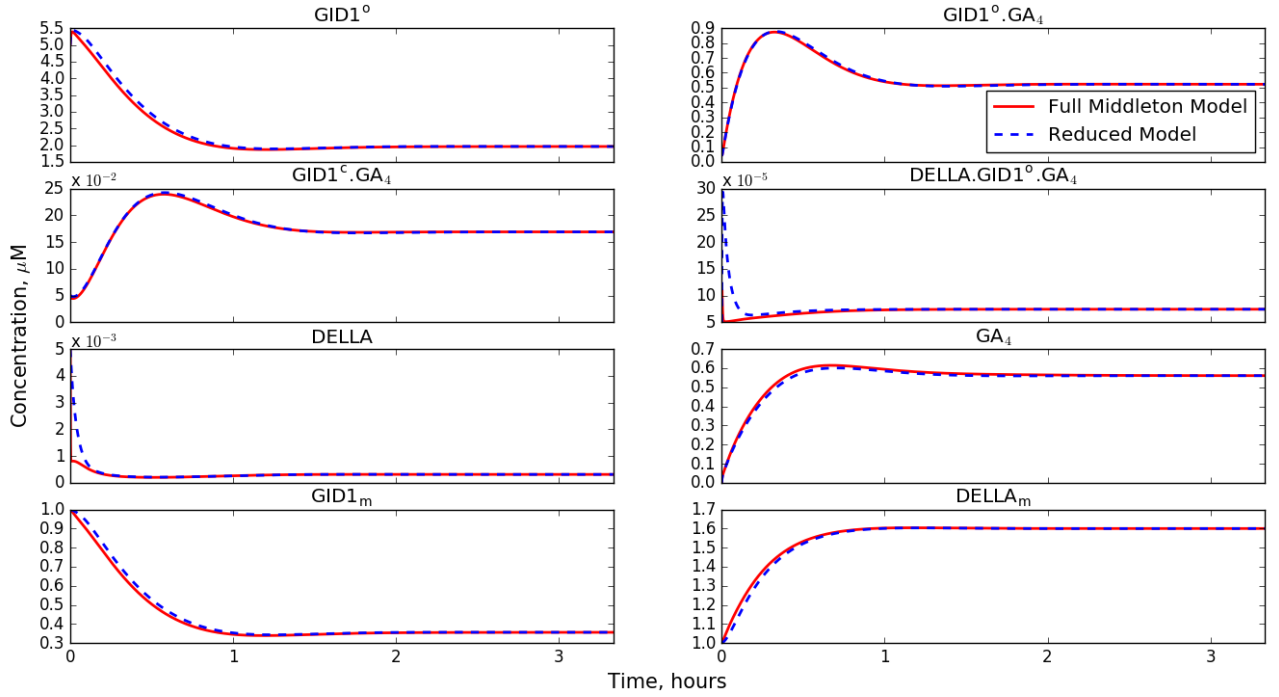


Figure 10: A comparison between the numerical simulations of the full model for the GA signalling pathway derived in [36], and the reduced model (10), (11) shows very good agreement.

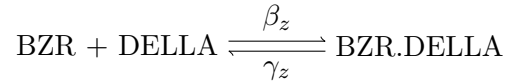


Figure 11: BR-GA crosstalk at the level of transcription factors, where BZR and DELLA form a complex.

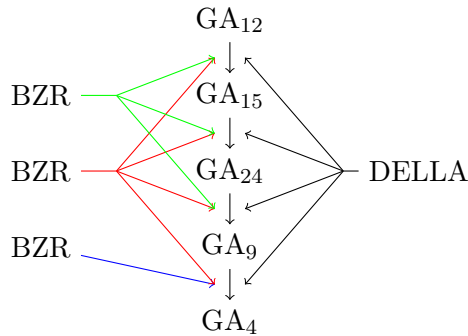


Figure 12: Proposed mechanisms for the influence of BZR on GA biosynthesis. The first model (green) comes from [33], where BZR influences the expression of GA20ox, in the second model (red) from [56] BZR affects both GA20ox and GA3ox expression, and in the third model (blue) from [53] BZR affects only GA3ox expression.

To derive the model for BR-GA crosstalk we coupled model (2) and model (10), (11) by adding new interaction terms describing the crosstalk mechanisms. Two terms were added, a term corresponding to the interaction of BZR and DELLA, which required the introduction of a new variable denoting the concentration of the complex BZR.DELLA, and a term corresponding to the BZR-mediated biosynthesis of GA. By varying the parameters of these new terms, we were then able to analyse the influence that each mechanism exert over the corresponding signalling processes.

BZR.DELLA complex formation is modelled as a reversible reaction between BZR and DELLA. The

concentration of BZR.DELLA is denoted by z_d , and the parameters β_z and γ_z denote the binding rate of BZR and DELLA and the dissociation rate of BZR.DELLA, respectively,

$$\frac{dz_d}{dt} = \beta_z z d_l - \gamma_z z_d. \quad (12)$$

From this we modify system (2) to take account of the dynamics of BZR.DELLA

$$\begin{aligned} \frac{db}{dt} &= \beta_k(R_{tot} - K_{tot} + k)k - \beta_b(K_{tot} - k)b + \frac{\alpha_b}{1 + (\theta_b z)^{h_b}} - \mu_b b, \\ \frac{dk}{dt} &= \beta_b(K_{tot} - k)b - \beta_k(R_{tot} - K_{tot} + k)k, \\ \frac{dz}{dt} &= \delta_z(Z_{tot} - z - z_d)k - \rho_z \frac{z}{1 + (\theta_z k)^{h_z}} - \beta_z z d_l + \gamma_z z_d. \end{aligned} \quad (13)$$

System (11) is modified by taking account of the dynamics of BZR.DELLA, and extending the Hill function describing GA biosynthesis to include BZR-mediated gene expression. For the crosstalk model we do not assume that exogenous GA is entering the system, hence the term $\phi_g(\omega_g - g)$ describing this process in (11) is removed. BZR is assumed to control gene expression in the same manner as DELLA, but with relative activity described by ϕ_z , where ϕ_z is the ratio between the binding thresholds of DELLA and BZR

$$\begin{aligned} \frac{dd_l}{dt} &= -\beta_d d_l r_g^c + \gamma_d r_d + \alpha_d d_m - \beta_z z d_l + \gamma_z z_d, \\ \frac{dg}{dt} &= \alpha_g \frac{(d_l + \phi_z z)^4}{\vartheta_g + (d_l + \phi_z z)^4} - \beta_g r g + \gamma_g r_g^o - \mu_g g. \end{aligned} \quad (14)$$

The values for the parameters β_z , γ_z governing the direct interaction between DELLA and BZR are estimates from values for similar complex formation and separation from [36]. We first assumed that the binding thresholds of BZR and DELLA were equal i.e. $\phi_z = 1$, and then analysed the influence of variation in ϕ_z on the dynamics of the solutions of (10), (12)-(14).

In order to analyse the relative effects of the different crosstalk mechanisms, we examined the behaviour of the model for different values of β_z , γ_z and ϕ_z . The model was solved numerically for four different conditions: no crosstalk ($\beta_z, \gamma_z, \phi_z = 0$), crosstalk via BZR activated GA biosynthesis only ($\beta_z, \gamma_z = 0$), crosstalk via BZR.DELLA complex formation only ($\phi_z = 0$), and crosstalk via both mechanisms, Fig. 13. Only for variables including GA were there any differences when including BZR-mediated biosynthesis of GA, and for all other variables there was close agreement between the cases of no crosstalk and crosstalk via biosynthesis only, and close agreement between the cases of crosstalk via complex formation only and crosstalk via both mechanisms. To examine the influences of both mechanisms on the BR and GA signalling pathways, the relevant parameters were varied. Variation in β_z and γ_z led to long-term behaviour changes for the components of the BR signalling pathway, and short-term changes for the components of the GA signalling pathway, Fig. 14. Variations in ϕ_z had very little effect with differences in behaviour in variables containing GA for the cases $\phi_z = 0$ and $\phi_z > 0$ (results omitted). From this we concluded that direct interaction between BZR and DELLA is the predominant form of crosstalk between the BR and GA signalling pathways.

In order to examine the effects of mutations in the BR signalling pathway upon BR-GA crosstalk, changes in parameters δ_z , ρ_z and θ_z are introduced into model (10), (12)-(14), Fig. 15. Damped oscillations in the dynamics of the components of the BR signalling pathway induced no such behaviour in the dynamics of the GA signalling pathway, and despite causing some changes in the early behaviour of the dynamics of the GA signalling pathway their long term behaviour remains similar. Alongside the induced perturbation in the BR signalling pathway, we also varied β_z and γ_z to examine how crosstalk affects the dynamics of both pathways in this case. We found in the case that β_z/γ_z is large, the dynamics of the BR signalling pathway are virtually unchanged from the cases with smaller values of β_z/γ_z , however the long-term behaviour of the GA signalling pathway was significantly effected, with all components except GA_4 and $DELLA_m$ having substantially different stationary solutions.

Given the observed large effect of crosstalk on the BR pathway as compared with the GA pathway, see Figs 13 and 14, we analysed how directly altering each pathway would affect the other, Fig. 16. We

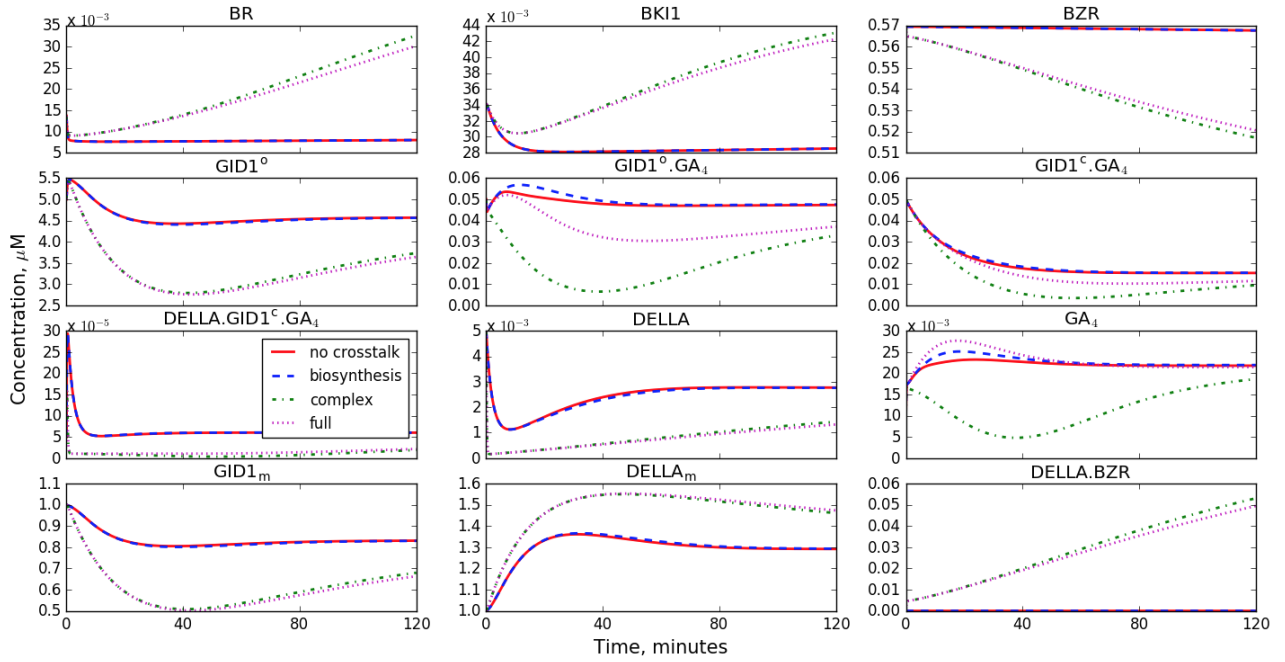


Figure 13: Comparisons between solutions of the crosstalk model (10), (12)-(14); ‘no crosstalk’ refers to the case where $\beta_z = \gamma_z = \phi_z = 0$; ‘biosynthesis’ refers to the case where the only crosstalk between the BR and GA signalling pathways is BZR-induced biosynthesis of GA ($\beta_z = \gamma_z = 0, \phi_z \neq 0$); ‘complex’ refers to the case where the only crosstalk between the BR and GA signalling pathways is complex formation of BZR and DELLA ($\beta_z, \gamma_z \neq 0, \phi_z = 0$); ‘full’ refers to the case where crosstalk between the BR and GA signalling pathways can be via both mechanisms BZR-mediated GA biosynthesis and complex formation of BZR and DELLA ($\beta_z, \gamma_z, \phi_z \neq 0$).

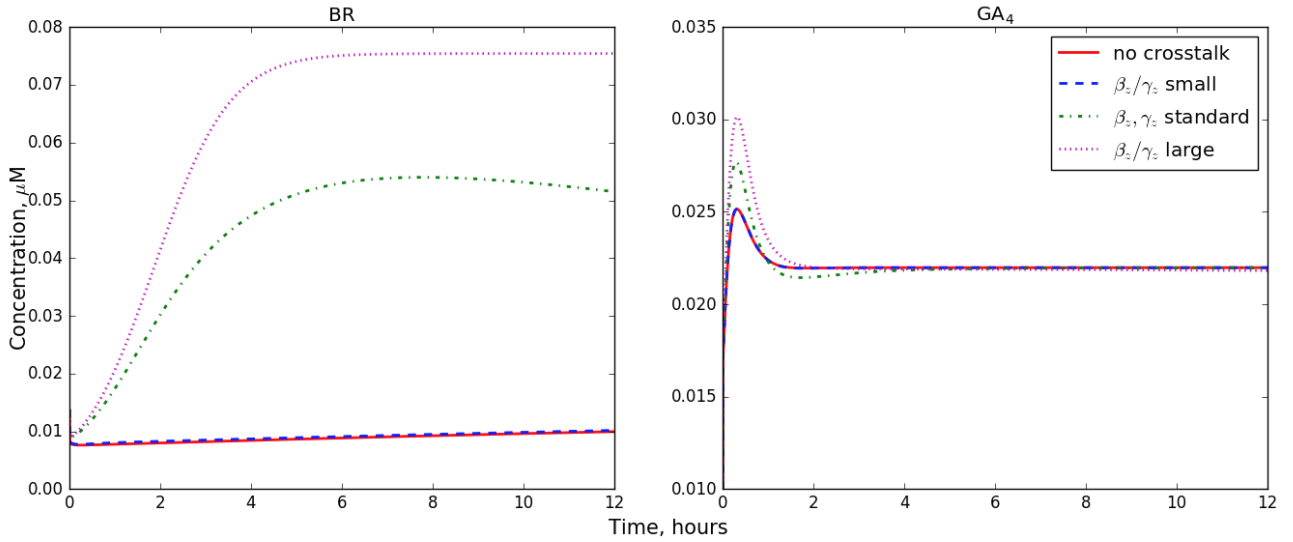


Figure 14: Variation of the values of β_z and γ_z suggests that the BR signalling pathway is more sensitive to the effects of crosstalk than the GA signalling pathway; ‘no crosstalk’ corresponds to the case $\beta_z = \gamma_z = 0$, ‘small’ the case where β_z/γ_z has order of magnitude zero, i.e. $\beta_z/\gamma_z \approx 0.75$, for ‘standard’ β_z/γ_z has order of magnitude two, i.e. $\beta_z/\gamma_z \approx 75$, and for ‘large’ β_z/γ_z has order of magnitude four, i.e. $\beta_z/\gamma_z \approx 7500$.

modelled the overexpression of BR and GA hormones by increasing parameters α_b and α_g . Overexpression of BR (increase of α_b) resulted in major changes in the BR signalling pathway with increases in the concentrations of BR, BKI1 and BZR, but almost negligible change in the GA signalling pathway. Overexpression of GA had more widespread effects, causing increases in the concentrations of

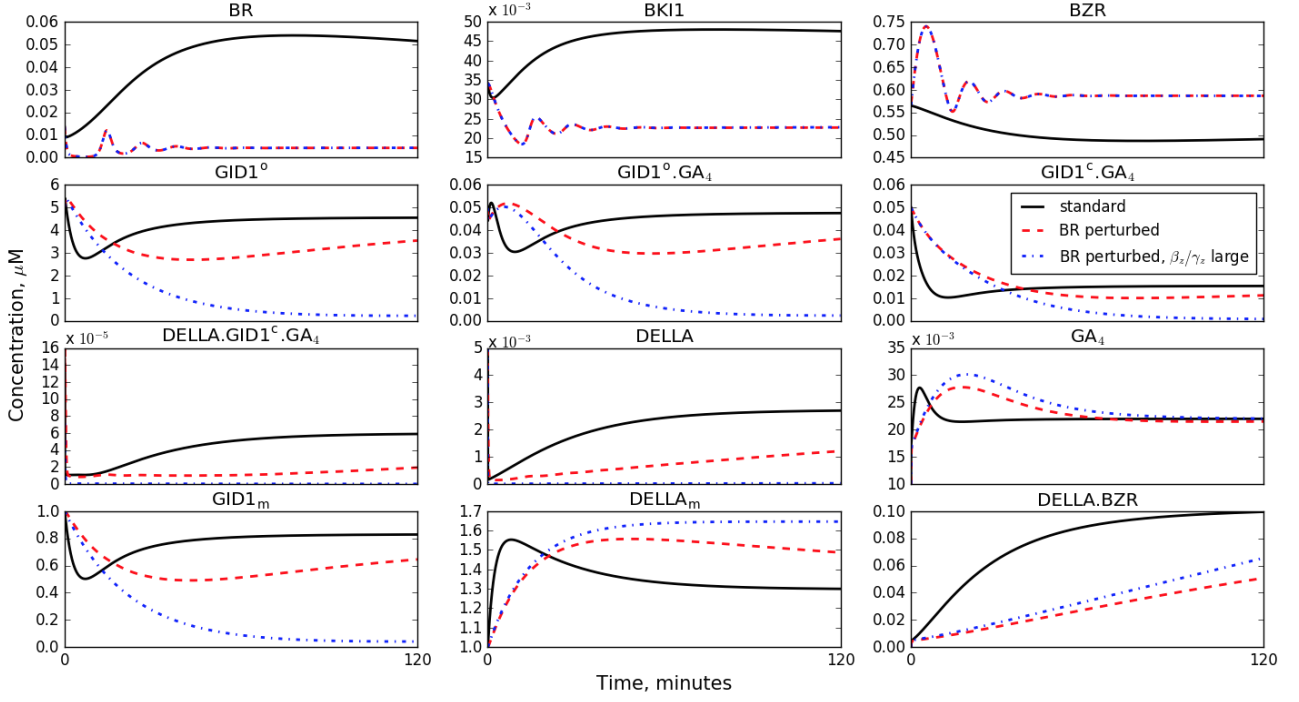


Figure 15: Oscillations in the BR pathway lead to short term changes in the dynamics of the GA pathway, and increasing β_z/γ_z causes more long term effects on the GA signalling pathway. In the ‘*standard*’ case all parameters are as in Tables 1 and 3 and $\beta_z = 10 \mu\text{M}^{-1}\text{min}^{-1}$, $\gamma_z = 0.133 \text{ min}^{-1}$. For the ‘*BR perturbed*’ case parameters δ_z and ρ_z have had their orders of magnitude increased by three, $\theta_z = 41.2\mu\text{M}^{-1}$, and all other parameters are as in Tables 1 and 3 and $\beta_z = 10$, $\gamma_z = 0.133$. The ‘*BR perturbed, β_z/γ_z large*’ has the same parameter values as the ‘*BR perturbed*’, however here β_z/γ_z has order of magnitude four, i.e. $\beta_z/\gamma_z \approx 7500$, similar to Fig. 14.

BZR, $\text{GID1}^o.\text{GA}_4$, $\text{GID1}^c.\text{GA}_4$, $\text{DELLA}.\text{GID1}^c.\text{GA}_4$ and GA_4 , and decreases in the concentrations of BR, BKI1, GID1^o , GID1_m and $\text{DELLA}.\text{BZR}$.

In all cases of BR-GA interactions discussed here we considered the parameter values for the BR signalling pathway model as in Table 1. However similar behaviours are observed also if considering the parameter values as in Table 2, hence we do not present the simulation results for those cases.

6.3 Modelling Spatial Heterogeneity in the Crosstalk Signalling

We also considered the spatial heterogeneity in the crosstalk model. Here, the coupled PDE-ODE model for the BR signalling pathway (7)-(9) was modified to include the components of the GA signalling pathway. GA was assumed to be able to diffuse freely throughout the cell, and all other components of the GA signalling pathway were assumed to be nuclear-localized. We retain the same assumptions for the components of the BR signalling pathway as in section 5. This led to a set of reaction-diffusion equations for BR, BKI1, BZR-p the same as in (7), and for GA:

$$\partial_t g = D_g \partial_x^2 g - \mu_g g \quad \text{in } \Omega_c. \quad (15)$$

We assume that receptor based interactions of BR, BKI1 and BRI1 remain the same as in (8), and no influx of exogenous GA on the plasma membrane:

$$-D_g \partial_x g = 0 \quad \text{on } \Gamma_c. \quad (16)$$

The production of BR, change in phosphorylation status of BZR, and interactions between BZR and DELLA occur in the plant cell nucleus and are modelled as flux boundary conditions and ODEs on

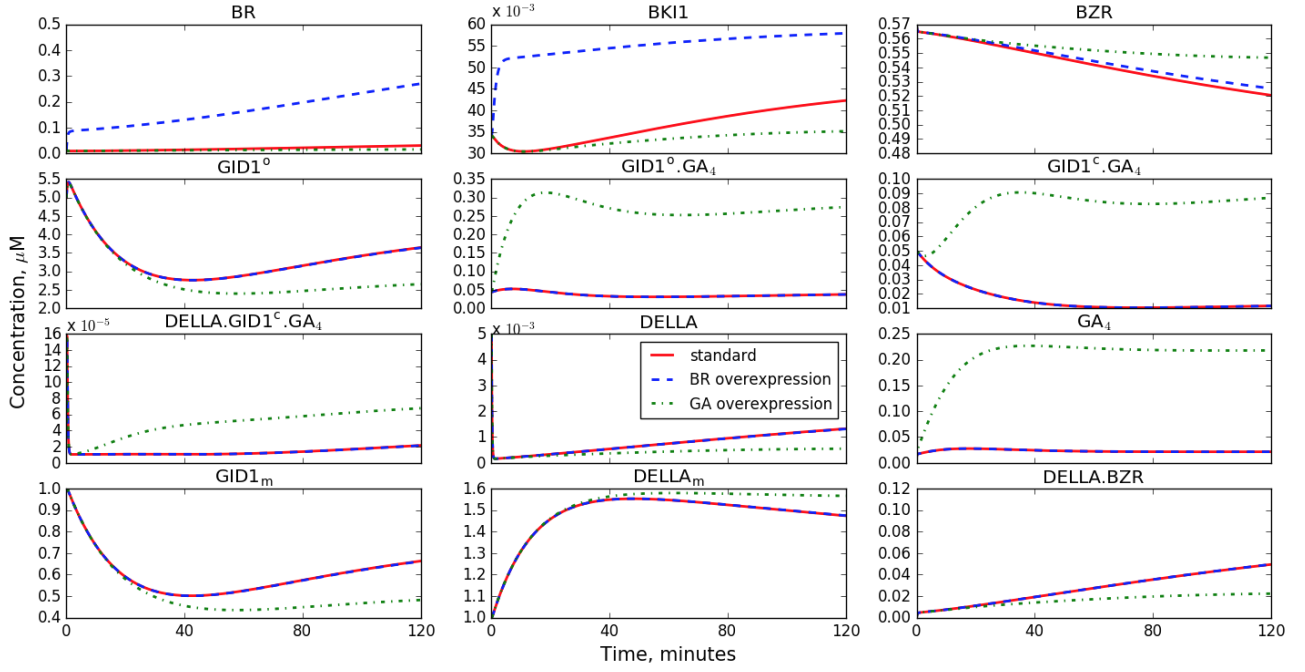


Figure 16: Examining the effects of hormonal overexpression on the dynamics of solutions of model (10), (12)-(14) for the crosstalk between the BR and GA signalling pathways. For the ‘*standard*’ case all parameters are as in Tables 1 and 3 and $\beta_z = 10 \mu\text{M}^{-1}\text{min}^{-1}$, $\gamma_z = 0.133 \text{ min}^{-1}$; in the ‘*BR overexpression*’ case, α_b ’s order of magnitude is increased by one; in the ‘*GA overexpression*’ case α_g ’s order of magnitude is increased by one.

the boundary Γ_n :

$$\left. \begin{aligned}
 D_b \partial_x b &= \frac{\tilde{\alpha}_b}{1 + (\tilde{\theta}_b z)^{h_b}} \\
 D_k \partial_x k &= 0 \\
 \frac{d\tilde{z}}{dt} &= \tilde{\delta}_z z_p k - \rho_z \frac{\tilde{z}}{1 + (\theta_z k)^{h_z}} - \tilde{\beta}_z \tilde{z} \tilde{d}_l + \gamma_z \tilde{z}_d \\
 D_z \partial_x z_p &= -\tilde{\delta}_z z_p k + \rho_z \frac{\tilde{z}}{1 + (\theta_z k)^{h_z}}
 \end{aligned} \right\} \text{ on } \Gamma_n. \quad (17)$$

All processes of the GA signalling pathway apart from degradation of GA are localised to the nucleus and are modelled by a system of ODEs for GID1^o , $\text{GA}_4.\text{GID1}^o$, $\text{GA}_4.\text{GID1}^c$, $\text{DELLA}.\text{GA}_4.\text{GID1}^c$,

DELLA, GID1_m and DELLA_m , and a flux boundary condition for GA on the boundary Γ_n :

$$\left. \begin{aligned}
 \frac{d\tilde{r}}{dt} &= -\beta_g \tilde{r}g + \gamma_g \tilde{r}_g^o + \tilde{\alpha}_r r_m - \mu_r r \\
 \frac{d\tilde{r}_g^o}{dt} &= \beta_g \tilde{r}g - (\gamma_g + \lambda^c) \tilde{r}_g^o + \lambda^o \tilde{r}_g^c \\
 \frac{d\tilde{r}_g^c}{dt} &= \lambda^c \tilde{r}_g^o - \lambda^o \tilde{r}_g^c - \tilde{\beta}_d \tilde{d}_l \tilde{r}_g^c + (\gamma_d + \mu_d) \tilde{r}_d \\
 \frac{d\tilde{r}_d}{dt} &= \tilde{\beta}_d \tilde{d}_l \tilde{r}_g^c - (\gamma_d + \mu_d) \tilde{r}_d \\
 \frac{d\tilde{d}_l}{dt} &= -\tilde{\beta}_d \tilde{d}_l \tilde{r}_g^c + \gamma_d \tilde{r}_d + \tilde{\alpha}_d d_m - \tilde{\beta}_z \tilde{z} \tilde{d}_l + \gamma_z \tilde{z}_d \\
 D_g \partial_x g &= \alpha_g \frac{(\tilde{d}_l + \phi_z \tilde{z})^4}{\tilde{\vartheta}_g + (\tilde{d}_l + \phi_z \tilde{z})^4} - \beta_g \tilde{r}g + \gamma_g \tilde{r}_g^o \\
 \frac{dr_m}{dt} &= \phi_r \left(\frac{\tilde{d}_l}{\tilde{\theta}_r + \tilde{d}_l} - r_m \right) \\
 \frac{dd_m}{dt} &= \phi_d \left(\frac{\tilde{\theta}_d}{\tilde{\theta}_d + \tilde{d}_l} - d_m \right)
 \end{aligned} \right\} \text{ on } \Gamma_n. \quad (18)$$

Finally crosstalk is modelled via formation of the BZR.DELLA complex

$$\frac{dz_d}{dt} = \beta_z z d_l - \gamma_z z_d \quad \text{on } \Gamma_n. \quad (19)$$

Similar to model (7)-(9), to ensure appropriate units we obtain rescaled relations between boundary-localised variables in model (15)-(19) and the corresponding variables in model (10), (12)-(14), i.e. $\tilde{r}_k = l_c r_k$, $\tilde{r}_b = l_c r_b$, $\tilde{z} = l_c z$, $\tilde{r} = l_c r$, $\tilde{r}_g^o = l_c r_g^o$, $\tilde{r}_g^c = l_c r_g^c$, $\tilde{r}_d = l_c r_d$, $\tilde{d}_l = l_c d_l$, and $\tilde{z}_d = l_c z_d$. Since r_m and d_m were already relative quantities with no units there was no need for them to be scaled. To balance units certain parameters also had to be rescaled: parameters α_b , δ_z , α_r , α_d , α_g , ϑ_r and ϑ_d from (10), (12)-(14) were all multiplied by l_c such that $\tilde{\alpha}_b = l_c \alpha_b$ etc.; θ_b , β_z and β_d were all divided by l_c such that $\tilde{\theta}_b = \theta_b / l_c$ etc.; and ϑ_g was scaled such that $\tilde{\vartheta}_g = l_c^4 \vartheta_g$. Since GA molecules have similar size to BR molecules, we consider $D_g = D_b$. All other parameters were taken to be the same as those used for model (10), (12)-(14), i.e. from Tables 1 and 3 and $\beta_z = 10 \mu\text{M}^{-1} \text{min}^{-1}$, $\gamma_z = 0.133 \text{min}^{-1}$.

System (7), (8), (15)-(19) was solved numerically, and these solutions were averaged over the space and then compared to the solutions of system (10), (12)-(14). The behaviour of the two models was similar for most of the parameter sets considered in section 6.2, see e.g. standard cases in Figs. 15 and 17, however spatially heterogeneous steady states are characteristic for model (7), (8), (15)-(19), see Fig. 18. Spatial heterogeneity does have a significant effect in the case where perturbations in the phosphorylation of BZR lead to damped oscillations in the BR signalling pathway, with much different behaviours of solutions of system (7), (8), (15)-(19) than for (10), (12)-(14), comparing Figs. 15 and 17. When the BR signalling pathway is ‘strongly perturbed’, i.e. δ_z and ρ_z are increased sufficiently high, the oscillations in the components of the BR signalling pathway also cause oscillatory behaviour in the components of the GA signalling pathway, suggesting that spatial heterogeneity may contribute to instability of solutions in extreme cases.

7 Discussion and Conclusion

Plants rely on complex integrated hormonal signalling pathways in order to respond and adapt to changing environmental conditions. The BR and GA signalling pathways have a diverse range of effects on plant growth and developmental processes, some of which overlap. To examine the behaviours of these signalling pathways and their interactions we developed mathematical models of the BR signalling pathway, and crosstalk between the BR and GA pathways under assumptions of both spatial homogeneity: models (1) and (10), (12)-(14), and spatial heterogeneity of signalling processes: models (7)-(9) and (7), (8), (15)-(19).

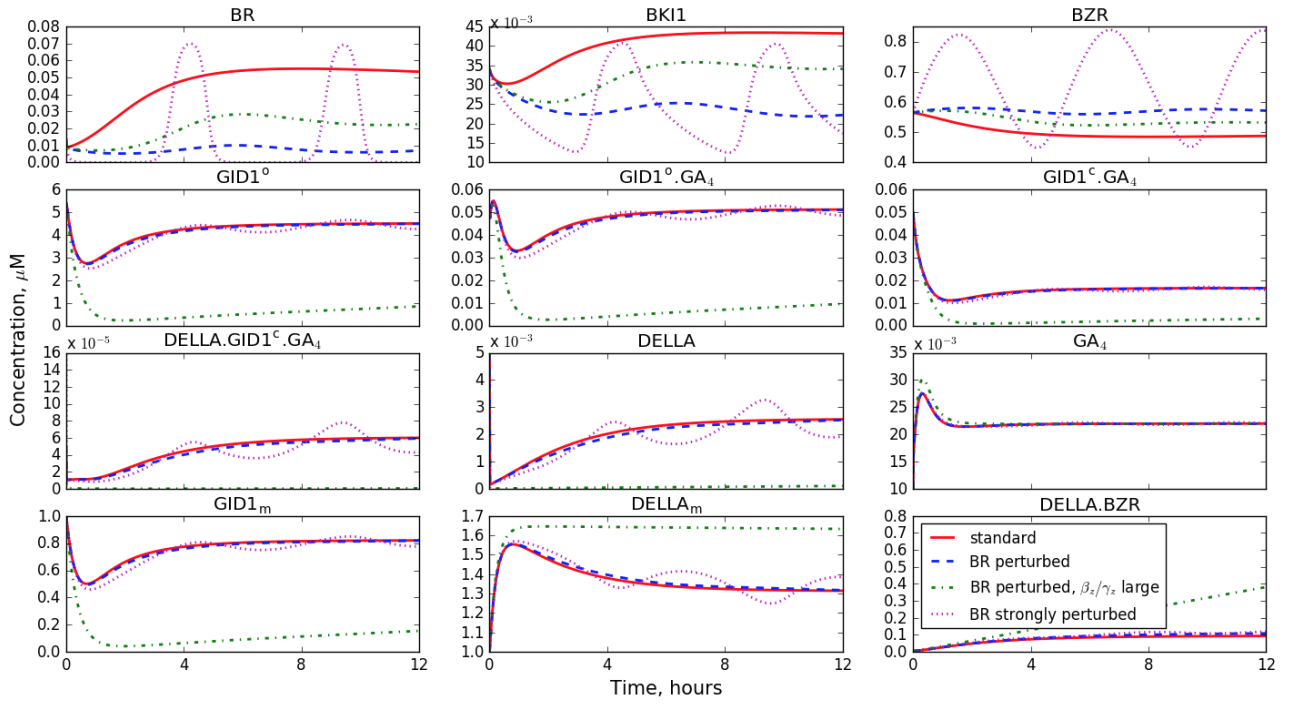


Figure 17: Solutions of system (7), (8), (15)-(19), averaged over space. For ‘*standard*’ parameter values are as in Tables 1 and 3 and $\beta_z = 10 \mu\text{M}^{-1}\text{min}^{-1}$, $\gamma_z = 0.133 \text{ min}^{-1}$. For both ‘*BR perturbed*’ and ‘*BR perturbed, β_z/γ_z large*’ δ_z and ρ_z have had their orders of magnitude increased by two, $\theta_z = 41.2\mu\text{M}^{-1}$, β_z/γ_z has order of magnitude four, i.e. $\beta_z/\gamma_z \approx 7500$, for ‘*BR perturbed, β_z/γ_z large*’ only, and all other parameters are as in Tables 1 and 3. For the case ‘*BR strongly perturbed*’ δ_z and ρ_z have had their orders of magnitude increased by three, $\theta_z = 41.2\mu\text{M}^{-1}$, all other parameters as in Tables 1 and 3 and $\beta_z = 10 \mu\text{M}^{-1}\text{min}^{-1}$, $\gamma_z = 0.133 \text{ min}^{-1}$.

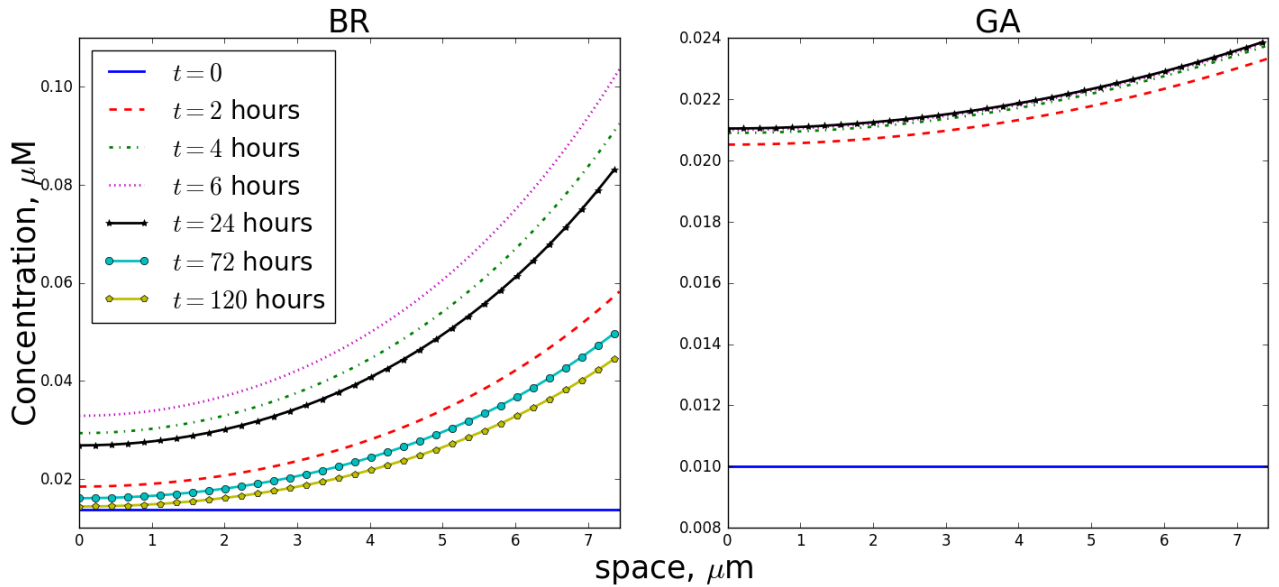


Figure 18: The spatial distribution of BR and GA in the cell segment Ω_c (solutions of (7), (8), (15)-(19)) at different times, parameter values are as in Tables 1 and 3 and $\beta_z = 10 \mu\text{M}^{-1}\text{min}^{-1}$, $\gamma_z = 0.133 \text{ min}^{-1}$. The concentration of BR starts of uniform, and is produced at $x = 7.43 \mu\text{m}$, the nucleus, leading to the greatest concentration at this point. The overall concentration increases over the first 8 h, but then decreases steadily, arriving at a spatially heterogeneous steady state after 120 h. The concentration of GA is also greater at $x = 7.43 \mu\text{m}$ where it is produced, but GA attains its spatially heterogeneous steady state after 24 h, much more quickly than BR.

The parameters in the model for the BR signalling pathway (2) were determined upon validating the model by comparing its numerical solutions to experimental data from [50]. Using numerical optimisation techniques we were able to get a good fit for the diverse data sets corresponding to the different growth conditions considered in [50]. Our calculations resulted in values for δ_z and ρ_z of a much lower order of magnitude than the rest of the parameters in the model, suggesting that the phosphorylation of BZR occurs on a much slower time scale than e.g. perception of BR by BRI1. The model parameters were optimised under two different constraints on the value of β_k , (4) and (5), corresponding to two different mechanisms governing the interactions of BR, BRI1, and BKI1, where BR and BKI1 binding to and dissociation from BRI1 is instantaneous, or a complex BR.BRI1.BKI1 can be formed, respectively. Most parameters had very similar or identical values, with the only notable differences being for (naturally) β_k , and the parameters governing the phosphorylation of BZR: δ_z , ρ_z . Overall our model fitted the data well for both mechanisms (4) and (5), with R^2 values of 0.89 and 0.92 respectively, suggesting that both of these mechanisms may accurately predict the dynamics of the BR signalling pathway. The only growth condition for which the model had a less accurate fit was for when the growth medium was supplemented with BL.

Qualitative analysis of system (6) revealed that it has only one steady state for the parameter space P , and that this steady state is stable in a neighbourhood of the parameter sets defined in Tables 1 and 2. Bifurcation analysis showed that for a bounded set of values of (δ_z, ρ_z) , with $\theta_z = 41.2 \mu\text{M}^{-1}$ and all other parameters as in Table 1, system (6) has periodic solutions, i.e. system (6) undergoes a Hopf bifurcation upon varying parameters δ_z , ρ_z , corresponding to the dephosphorylation rate and phosphorylation rate of BZR respectively. No such bifurcations were found when considering a large range of values for δ_z , ρ_z , and $\theta_z = 41.2 \mu\text{M}^{-1}$ and all other parameters as in Table 2. However, since the values of δ_z , ρ_z for which a bifurcation exists are likely to be biologically unrealistic as they are much greater than the values yielded by validation of the model by experimental data, this suggests that within some range of normal function the BR signalling pathway has good stability, which is of crucial importance for proper function of plant tissues. Results also suggest that if BR and BKI1 associate and dissociate from BRI1 instantaneously, as in mechanism (4), stability of the pathway is principally dependent upon the phosphorylation state of BZR. Further if BR.BRI1.BKI1 can be formed, as in mechanism (5), stability of solutions to model (6) for a wide range of all parameters ensures effective BR homeostasis.

Numerical solutions for the spatially heterogeneous model (7)-(9) averaged over space and ODE model (2) for the BR signalling pathway demonstrated similar behaviours for the parameter sets when the solutions of (7)-(9) and of (2) converge to the steady state as $t \rightarrow \infty$. In the oscillatory parameter regime discussed in section 4.1, the PDE-ODE model exhibited distinct behaviour to the ODE model, Fig. 8, suggesting that under such conditions the spatial heterogeneity of the signalling pathway has a large influence on the dynamics of the molecules involved in the BR signalling pathway.

We investigated the effects of interactions between the BR and GA signalling pathways and the BR-GA signalling crosstalk mechanisms [31, 53, 56] by coupling (2), (10) and (11) to obtain model (10), (12)-(14), in order to establish which mechanism is more biologically significant [40, 52, 57]. We examined the effects of BZR-mediated biosynthesis of GA and of BZR.DELLA complex formation on the behaviour of the BR and GA signalling pathways. We modelled the cases where there was: no crosstalk, BZR-mediated biosynthesis of GA only, BZR.DELLA complex formation only, and both BZR-mediated biosynthesis of GA and BZR.DELLA complex formation. The cases of no crosstalk and BZR-mediated biosynthesis exhibited similar behaviour to each other, and the cases of BZR.DELLA complex formation and both BZR-mediated biosynthesis of GA and BZR.DELLA complex formation exhibited similar behaviour to each other, Fig. 13. Further, upon variation of the ratio between DELLA and BZR binding thresholds ϕ_z the change in behaviour of most components of both pathways was negligible, whereas the variations in BZR.DELLA binding β_z and dissociation γ_z rates had a strong effect upon the BR signalling pathway, Fig. 14. From this we concluded that BZR.DELLA complex formation has a greater effect on the behaviour of the BR and GA signalling pathways. This

suggests that interactions between BZR and DELLA exert more influence over the dynamics of the pathways than BZR-mediated biosynthesis of GA and are more likely to be able to promote any effective change in the behaviour of the signalling processes. Numerical results also demonstrated that for all parameter sets where solutions tended to a steady state, the solutions of model (10), (12)-(14) and the averaged over space solutions of model (7), (8), (15)-(19) exhibit similar dynamics, although spatially heterogeneous steady-states are obtained for BR and GA concentrations, Fig. 18.

To examine whether disturbance of one signalling pathway had a greater effect on the other, we modelled the effects of overexpression of both BR and GA. Overexpression of BR resulted in large changes in the dynamics of the components of the BR signalling pathway only, and overexpression of GA resulted in large changes in the dynamics of the components of the GA signalling pathway, and small changes in the dynamics of the components of the BR signalling pathway, Fig. 16. In addition variation of β_z and γ_z led to large changes in the dynamics of the BR pathway but only short term changes in the dynamics of the GA pathway. From this we concluded that in general perturbations in the GA signalling pathway have greater influence on the BR signalling pathway than vice versa.

To examine the effects of mutations in the BR signalling pathway on the GA pathway, models (10), (12)-(14) and (7), (8), (15)-(19) were solved numerically considering different values for the parameters δ_z and ρ_z governing BZR phosphorylation. For the components of the GA signalling pathway solutions to the ODE model showed different short-term behaviour but tended to the same steady state, whereas the components of the BR signalling pathway tended to different steady state. If varying β_z and γ_z such that β_z/γ_z was large in the case when we have damped oscillation in the components of the BR signalling pathway, the dynamics of some of the components of the GA signalling pathway were significantly altered but the dynamics of the components of the BR signalling pathway were unchanged, Fig. 15. For the spatially heterogeneous model (7), (8), (15)-(19), in the oscillatory parameter regime oscillations in the BR signalling pathway propagated into the GA signalling pathway, Fig. 17. From this we conclude that only in the case where there is disturbance in both the BR signalling pathway and the mechanism of crosstalk between the BR and GA signalling pathways the dynamics of molecules in the BR signalling pathway have greater influence on the dynamics of molecules in the GA signalling pathway. This, together with the results discussed in the previous paragraph, suggests that under normal crosstalk the stability of individual signalling pathways is maintained even if there are disturbances in the other pathway.

To conclude, our analysis of new mathematical models for BR signalling pathway and the crosstalk between the BR and GA signalling pathways, derived here, provide a better understanding of the dynamics of signalling processes, dependent on model parameters and spatial heterogeneity. Our results for the BR signalling pathway highlight its stability, and suggest that this stability is particularly dependent on the mechanisms governing the phosphorylation state of BZR and the subcellular locations of these processes. Our results suggest that direct interaction between BZR and DELLA exerts a larger influence on the dynamics of the BR and GA signalling pathways than BZR-mediated biosynthesis of GA, and hence may be the primary mechanism of crosstalk between the two pathways. Our analysis indicates that during normal plant function, the GA signalling pathway exerts more influence over the BR signalling pathway than BR on GA, but mutations in the BR signalling pathway cause BR signalling to exert some short time influence over GA pathway and greater influence when coupled with disturbances in the crosstalk mechanism. Both BR signalling and crosstalk between BR and GA signalling are important for plant growth and development. Our modelling and analysis results also can be used to model the interactions between growth and signalling processes in order to better understand the influence of the BR and GA signalling pathways on growth and developmental processes in plants.

Acknowledgments

H.R. Allen gratefully acknowledges the support of an EPSRC DTA PhD studentship, research of M. Ptashnyk was partially supported by the EPSRC First Grant EP/K036521/1.

References

References

- [1] Patrick Achard and Pascal Genschik. Releasing the brakes of plant growth: how gas shutdown della proteins. *Journal of Experimental Botany*, 60(4):1085–1092, 2009.
- [2] Patrick Achard, Fan Gong, Soizic Cheminant, Malek Alioua, Peter Hedden, and Pascal Genschik. The cold-inducible cbf1 factordependent signaling pathway modulates the accumulation of the growth-repressing della proteins via its effect on gibberellin metabolism. *The Plant Cell*, 20:2117–2129, 2008.
- [3] Golam J. Ahammed, Xiao-Jian Xia, Xin Li, Kai Shi, Jing-Quan Yu, and Yan-Hong Zhou. Role of brassinosteroids in plant adaptation to abiotic stresses and its interplay with other hormones. *Current Protein & Peptide Science*, 16(5):462–473, 2015.
- [4] Catherine Albrecht, Freddy Boutrot, Cécile Segonzac, Benjamin Schwessinger, Selena Gimenez-Ibanez, Delphine Chinchilla, John P. Rathjen, Sacco C. de Vries, and Cyril Zipfel. Brassinosteroids inhibit pathogen-associated molecular pattern-triggered immune signaling independent of the receptor kinase bak1. *PNAS*, 109(1):303–308, 2012.
- [5] Herbert Amann. *Ordinary Differential Equations: An Introduction to Nonlinear Analysis*. de Gryuter, illustrated edition, 1990.
- [6] Ming-Yi Bai, Jian-Xiu Shang, Eunkyoo Oh, Min Fan, Yang Bai, Rodolfo Zentella, Tai ping Sun, and Zhi-Yong Wang. Brassinosteroid, gibberellin and phytochrome impinge on a common transcription module in arabidopsis. *Nature Cell Biology*, 14(8):810–817, 2012.
- [7] Andrzej Bajguz and Shamsul Hayat. Effects of brassinosteroids on the plant responses to environmental stresses. *Plant Physiology and Biochemistry*, 47:1–8, 2009.
- [8] Youssef Belkhadir and Yvon Jaillais. The molecular circuitry of brassinosteroid signaling. *New Phytologist*, 206:522–540, 2015.
- [9] Thomas Bouquin, Carsten Meier, Randy Foster, Mads Eggert Nielsen, and John Mundy. Control of specific gene expression by gibberellin and brassinosteroid. *Plant Physiology*, 127:450–458, 2001.
- [10] Manuella Catterou, Frédéric Dubois, Hubert Schaller, Laurent Aubanelle, Beate Vilmot, Brigitte S. Sangwan-Norreel, and Rajbir S. Sangwan. Brassinosteroids, microtubules and cell elongation in arabidopsis thaliana. ii. effects of brassinosteroids on microtubules and cell elongation in the bull mutant. *Planta*, 212:673–683, 2001.
- [11] Yuhee Chung and Sunghwa Choe. The regulation of brassinosteroid biosynthesis in arabidopsis. *Critical Reviews in Plant Sciences*, 32:396–410, 2013.
- [12] Steven D. Clouse. Molecular genetic studies confirm the role of brassinosteroids in plant growth and development. *The Plant Journal*, 10(1):1–8, 1996.
- [13] Steven D. Clouse. Brassinosteroid signal transduction: From receptor kinase activation to transcriptional networks regulating plant development. *The Plant Cell*, 23:1219–1230, 2011.

- [14] Steven D. Clouse. A history of brassinosteroid research from 1970 through 2005: Thirty-five years of phytochemistry, physiology, genes, and mutants. *Journal of Plant Growth Regulation*, 34:828–844, 2015.
- [15] Steven D. Clouse and Jenneth M. Sasse. Brassinosteroids: Essential regulators of plant growth and development. *Annual Review of Plant Physiology and Plant Molecular Biology*, 49:427–451, 1998.
- [16] Ellen H. Colebrook, Stephen G. Thomas, Andrew L. Phillips, and Peter Hedden. The role of gibberellin signalling in plant responses to abiotic stress. *Journal of Experimental Biology*, 217:67–75, 2014.
- [17] Jean-Michel Davière and Patrick Achard. Gibberellin signalling in plants. *Development*, 140(6):1147–1151, 2013.
- [18] National Center for Biotechnology Information. Pubchem compound database, cid=115196. <https://pubchem.ncbi.nlm.nih.gov/compound/115196>. (accessed July 24, 2017).
- [19] David Frigola, Ana I. Caño-Delgado, and Marta Ibañes. Methods for modeling brassinosteroid-mediated signaling in plant development. In Eugenia Russinova and Ana I. Caño-Delgado, editors, *Methods for Modeling Brassinosteroid-Mediated Signaling in Plant Development*, chapter 9, pages 103–120. Humana Press, New York, NY, 2017.
- [20] Javier Gallego-Bartolomé, Eugenio G. Minguet, Federico Grau-Enguix, Mohamad Abbas, Antonella Locascio, Stephen G. Thomas, David Alabadí, and Miguel A. Blásquez. Molecular mechanism for the interaction between gibberellin and brassinosteroid signaling pathways in arabidopsis. *PNAS*, 109(33):13446–13451, 2012.
- [21] Lorna J. Gibson. The hierarchical structure and mechanics of plant materials. *Journal of the Royal Society Interface*, 9:2749–2766, 2012.
- [22] Sean P. Gordon, Vijay S. Chickarmane, Carolyn Ohno, and Elliot M. Meyerowitz. Multiple feedback loops through cytokinin signaling control stem cell number within the arabidopsis shoot meristem. *PNAS*, 106(38):16529–16534, 2009.
- [23] Damian Gruszka. The brassinosteroid signaling pathway - new key players and interconnections with other signaling networks crucial for plant development and stress tolerance. *International Journal of Molecular Sciences*, 14:8740–8774, 2013.
- [24] Brian D. Hassard, Nicholas D. Kazarinoff, and Yieh-Hei Wan. *Theory and Applications of the Hopf Bifurcation*. Cambridge University Press, first edition, 1981.
- [25] Marta Ibañes, Norma Fabrègas, Joanne Chory, and Ana I. Caño-Delgado. Brassinosteroid signaling and auxin transport are required to establish the periodic pattern of arabidopsis shoot vascular bundles. *PNAS*, 106(32):13630–13635, 2009.
- [26] Eric Jones, Travis Oliphant, Pearu Peterson, et al. SciPy: Open source scientific tools for Python, 2001–. [Online; accessed 2017-02-13].
- [27] Tae-Wuk Kim, Marta Michniewicz, Dominique C. Bergmann, and Zhi-Yong Wang. Brassinosteroid regulate stomatal development by gsk3-mediated inhibition of a mapk pathway. *Nature*, 482:419–422, 2012.
- [28] Tae-Wuk Kim and Zhi-Yong Wang. Brassinosteroid signal transduction from receptor kinases to transcription factors. *Annual Review of Plant Biology*, 61:681–704, 2010.
- [29] Jianming Li and Joanne Chory. A putative leucine-rich repeat receptor kinase involved in brassinosteroid signal transduction. *Cell*, 90:929–938, 1997.

- [30] Lei Li and Xing Wang Deng. It runs in the family: regulation of brassinosteroid signaling by the *bzr1-bes1* class of transcription factors. *Trends in Plant Science*, 10(6):266–268, 2005.
- [31] Qian-Feng Li and Jun-Xian He. Mechanisms of signaling crosstalk between brassinosteroids and gibberellins. *Plant Signaling and Behaviour*, 8(7):e24686, 2013.
- [32] Qian-Feng Li, Chunming Wang, Lei Jiang, Shuo Li, Samuel S. M. Sun, and Jun-Xian He. An interaction between *bzr1* and *dellas* mediates direct signaling crosstalk between brassinosteroids and gibberellins in *arabidopsis*. *Science Signaling*, 5(244):ra72, 2012.
- [33] Jodi L. Stewart Lilley, Yinbo Gan, Ian A. Graham, and Jennifer L. Nemhauser. The effects of *dellas* on growth change with developmental stage and brassinosteroid levels. *The Plant Journal*, 76:165–173, 2013.
- [34] Junli Liu, Shaher Mehdi, Jennifer Topping, Petr Tarkowski, and Keith Lindsey. Modelling and experimental analysis of hormonal crosstalk in *arabidopsis*. *Molecular Systems Biology*, 6(373), 2010.
- [35] Alistair M. Middleton, John R. King, Malcolm J. Bennett, and Markus R. Owen. Mathematical modelling of the *aux/iaa* negative feedback loop. *Bulletin of Mathematical Biology*, 72:1383–1407, 2010.
- [36] Alistair M. Middleton, Susana Úbeda Tomás, Jayne Griffiths, Tara Holman, Peter Hedden, Stephen G. Thomas, Andrew L. Phillips, Michael J. Holdsworth, Malcolm J. Bennett, John R. King, and Markus R. Owen. Mathematical modelling elucidates the role of transcriptional feedback in gibberellin signaling. *PNAS*, 109(19):7571–7576, 2012.
- [37] Daniele Muraro, Helen Byrne, John King, Ute Voß, Joseph Kieber, and Malcolm Bennett. The influence of cytokinin/auxin cross-regulation on cell-fate determination in *arabidopsis thaliana* root development. *Journal of Theoretical Biology*, 283:152–167, 2011.
- [38] Carsten Müssig, Ga-Hee Shin, and Thoas Altmann. Brassinosteroids promote root growth in *arabidopsis*. *Plant Physiology*, 133(3):1261–1271, 2003.
- [39] Stephan Piotrowski and Michael Carus. Multi-criteria evaluation of lignocellulosic niche crops for use in biorefinery processes. Technical report, nova-Institut GmbH, Hürth, Germany, 2011.
- [40] John J. Ross and Laura J. Quittenden. Interactions between brassinosteroids and gibberellins: Synthesis or signaling? *The Plant Cell*, 28:829–832, 2016.
- [41] Hojin Ryu, Kangmin Kim, Hyunwoo Cho, and Ildoo Hwang. Predominant actions of cytosolic *bsu1* and nuclear *bin2* regulate subcellular localization of *bes1* in brassinosteroid signaling. *Molecules and Cells*, 29:291–296, 2010.
- [42] Hojin Ryu, Kangmin Kim, Hyunwoo Cho, Joonghyuk Park, Sunghwa Choe, and Ildoo Hwang. Nucleocytoplasmic shuttling of *bzr1* mediated by phosphorylation is essential in *arabidopsis* brassinosteroid signaling. *The Plant Cell*, 19:2749–2762, 2007.
- [43] Martial Sankar, Karen S. Osmont, Jakub Rolcik, Bojan Gujas, Danuse Tarkowska, Miroslav Strnad, Ioannis Xenarios, and Christian S. Hardtke. A qualitative continuous model of cellular auxin and brassinosteroid signaling and their crosstalk. *Bioinformatics*, 27(10):1404–142, 2011.
- [44] Ji She, Zhifu Han, Tae-Wuk Kim, Jinjing Wang, Wei Cheng, Junbiao Chang, Shuai Shi, Jiawei Wang, Maojun Yang, Zhi-Yong Wang, and Jijie chai. Structural insight into brassinosteroid perception by *bri1*. *Nature*, 474:472–476, 2011.
- [45] Asako Shimada, Miyako Ueguchi-Tanaka, Toru Nakatsu, Masatoshi Nakajima, Youichi Naoe, Hiroko Ohmiya, Hiroaki Kato, and Makoto Matsuoka. Structural basis for gibberellin recognition by its receptor *gid1*. *Nature*, 456:520–523, 2008.

- [46] Yukihiisa Shimada, Shozo Fujioka, Narumasa Miyauchi, Masayo Kushiro, Suguru Takatsuto, Takahita Nomura, Takao Yokota, Yuji Kamiya, Gerard J. Bishop, and Shigeo Yoshida. Brassinosteroid-6-oxidases from arabidopsis and tomato catalyse multiple c-6 oxidations in brassinosteroid biosynthesis. *Plant Physiology*, 126(2):770–779, 2001.
- [47] Lucyna Sieminska, Matthew Ferguson, Tadeusz Waldeck Zerda, and Ernest Couch. Diffusion of steroids in porous sol-gel glass: Application in slow drug delivery. *Journal of Sol-Gel Science and Technology*, 8:1105–1109, 1997.
- [48] Marc Sturrock, Alan J. Terry, Dimitris P. Xirodimas, Alastair M. Thompson, and Mark A.J. Chaplain. Spatio-temporal modelling of the hes1 and p53-mdm2 intracellular signalling pathways. *Journal of Theoretical Biology*, 273:15–31, 2011.
- [49] Yu Sun, Xi-Ying Fan, Dong-Mei Cao, Wenqiang Tang, Jia-Ying Zhu, Jun-Xian He, Ming-Yi Bai, Shengwai Zhu, Eunkyoo Oh, Sunita Patil, Tae-Wuk Kim, Hongkai Ji, Wing Hong Wong, Seung Y. Rhee, and Zhi-Yong Wang. Integration of brassinosteroid signal transduction with the transcription network for plant growth regulation in arabidopsis. *Developmental Cell*, 19:765–777, 2010.
- [50] Kiwamu Tanaka, Tadao Asami, Shigeo Yoshida, Yasushi Nakamura, Tomoaki Matsuo, and Shige-hisa Okamoto. Brassinosteroid homeostasis in arabidopsis is ensured by feedback expressions of multiple genes involved in its metabolism. *Plant Physiology*, 138:1117–1125, 2005.
- [51] Kiwamu Tanaka, Yasushi Nakamura, Tadao Asami, Shigeo Yoshida, Tomoaki Matsuo, and Shige-hisa Okamoto. Physiological roles of brassinosteroids in early growth of arabidopsis: Brassinosteroids have a synergistic relationship with gibberellin as well as auxin in light-grown hypocotyl elongation. *Journal of Plant Growth Regulation*, 22:259–271, 2003.
- [52] Hongning Tong and Chengcai Chu. Reply: Brassinosteroid regulates gibberellin synthesis to promote cell elongation in rice: Critical comments on ross and quittenden’s letter. *The Plant Cell*, 28:833–835, 2016.
- [53] Hongning Tong, Yunhua Xiao, Dapu Liu, Shaopei Gao, Linchuan Liu, Yanhai Yin, Yun Jin, Qian Qian, and Chengcai Chu. Brassinosteroid regulates cell elongation by modulating gibberellin metabolism in rice. *The Plant Cell*, 26:4376–4393, 2014.
- [54] Susana Úbeda Tomás, Fernán Federici, Ilda Casimiro, Gerrit T.S. Beemster, Rishikesh Bhalerao, Ranjan Swarup, Peter Doerner, Jim Haseloff, and Malcolm J. Bennett. Gibberellin signaling in the endodermis controls arabidopsis root meristem size. *Current Biology*, 19:1194–1199, 2009.
- [55] Miyako Ueguchi-Tanaka, Motoyuki Ashikari, Masatoshi Nakajima, Hironori Itoh, Etsuko Katoh, Masatomo Kobayashi, Ten yuan Chow, Yue ie C. Hsing, Hidemi Kitano, Isomaro Yamaguchi, and Makoto Matsuoka. Gibberellin insensitive dwarf1 encodes a soluble receptor for gibberellin. *Nature*, 437:693–698, 2005.
- [56] Simon J. Unterholzner, Wilfried Rozhon, Michael Papacek, Jennifer Ciomas, Theo Lange, Karl G. Kugler, Klaus F. Mayer, Tobias Sieberer, and Brigitte Poppenberger. Brassinosteroids are master regulators of gibberellin biosynthesis in arabidopsis. *The Plant Cell*, 27:2261–2272, 2015.
- [57] Simon J. Unterholzner, Wilfried Rozhon, and Brigitte Poppenberger. Reply: Interaction between brassinosteroids and gibberellins: Synthesis or signaling? in arabidopsis, both! *The Plant Cell*, 28:836–839, 2016.
- [58] G.Wilma van Esse, Simon van Mourik, Hans Stigter, Colette A. ten Hove, Jaap Molenaar, and Sacco C. de Vries. A mathematical model for brassinosteroid insensitive1-mediated signaling in root growth and hypocotyl elongation. *Plant Physiology*, 160:523–532, 2012.

- [59] G. Wilma van Esse, Adrie H. Westphal, Ramya Preethi Surendran, Catherine Albrecht, Boudewijn van Veen, Jan Willem Borst, and Sacco C. de Vries. Quantification of the brassinosteroid insensitive 1 receptor in planta. *Plant Physiology*, 156:1691–1700, 2011.
- [60] Josep Vilarrasa-Blasi, Mary-Paz González-García, David Frigola, Norma Fàbregas, Konstantinos G. Alexiou, Nuria López-Bigas, Susana Rivas, Alain Jauneau, Jan U. Lohmann, Philip N. Benfey, Marta Ibañes, and Ana I. Caño-Delgado. Regulation of plant stem cell quiescence by a brassinosteroid signaling module. *Developmental Cell*, 30:36–47, 2014.
- [61] Jie Wang, Jianjun Jiang, Jue Wang, Lei Chen, Shi-Long Fan, Jia-Wei Wu, Xuelu Wang, and Zhi-Xin Wang. Structural insights into the negative regulation of bri1 signaling by bri1-interacting protein bki1. *Cell Research*, 24:1328–1341, 2014.
- [62] Lu Wang, Chunfeng Duan, Dapeng Wu, and Yafeng Guan. Quantification of endogenous brassinosteroids in sub-gram plant tissues by in-line matrix solid-phase dispersion-tandem solid phase extraction coupled with high performance liquid chromatography-tandem mass spectrometry. *Journal of Chromatography A*, 1359:44–51, 2014.
- [63] Wenfei Wang, Ming-Yi Bai, and Zhi-Yong Wang. The brassinosteroid signaling network - a paradigm of signal integration. *Current Opinion in Plant Biology*, 21:147–153, 2014.
- [64] Zhi-Yong Wang, Hideharu Seto, Shozo Fujioka, Shigeo Yoshida, and Joanne Chory. Bri1 is a critical component of a plasma-membrane receptor for plant steroids. *Nature*, 410:380–383, 2001.
- [65] Shinjiro Yamaguchi. Gibberellin metabolism and its regulation. *The Annual Review of Plant Biology*, 59:225–251, 2008.
- [66] Cang-Jin Yang, Chi Zhang, Yang-Ning Lu, Jia-Qi Jin, and Xue-Lu Wang. The mechanisms of brassinosteroids’ action: From signal transduction to plant development. *Molecular Plant*, 4(4):588–600, 2011.
- [67] Jia-Ying Zhu, Juthamas Sae-Seaw, and Zhi-Yong Wang. Brassinosteroid signalling. *Development*, 140(8):1615–1620, 2013.

A Validation of model (2) against experimental data

To improve the optimisation process for parameter estimation we calculated additional constraints for some parameter values using experimental data.

We first calculated the level of endogenous BL using a value of 5.26 ng g⁻¹ (the midpoint of the reported range in mature plants) which was obtained from [62]. In order to convert this into an appropriate value in units of μM, we first need the density of plant material. We estimate this by noting that the density of cellulose is 1.5 kg L⁻¹ [21], and that cellulose constitutes approximately 50% of plant material [39]. For the outstanding amount, we make an assumption that rest of the material is largely accounted for by cytoplasm, which we assume to have an approximately equal density to water, i.e. 1 kg L⁻¹. From this we get an estimate of 1.25 kg L⁻¹ for the density of plant material. Finally the molecular weight of BL is 480.686 g mol⁻¹ [18]. From this data we calculate the endogenous BR concentration as

$$\begin{aligned} \frac{\text{quantity} \times \text{density}}{\text{molecular weight}} &= \frac{(5.26 \times 10^{-6} \text{ g kg}^{-1}) \times (1.25 \text{ kg L}^{-1})}{480.686 \text{ g mol}^{-1}} \\ &= 0.0137 \times 10^{-6} \text{ mol L}^{-1} = 13.7 \times 10^{-3} \text{ } \mu\text{M}. \end{aligned}$$

We denote this new constant by $[BR]_0$, and assume it to be the steady state concentration of BR. We write μ_b in terms of α_b , θ_b , δ_z , Z_{tot} , ρ_z , θ_z and h_z by considering the steady state solution of (2):

$$\mu_b = \frac{\alpha_b}{[BR]_0 \left(1 + \left(\theta_b \frac{Z_{tot} \delta_z [BKI1]_0 (1 + (\theta_z [BKI1]_0)^{h_z})}{\rho_z + \delta_z [BKI1]_0 (1 + (\theta_z [BKI1]_0)^{h_z})} \right)^{h_b} \right)},$$

where $[BKI1]_0$ denotes the steady state concentration of BKI1, which can be calculated using $[BR]_0$.

We adopt two approaches for the calculation of $[BKI1]_0$ and β_k . First we consider the BR.BRI1 dissociation constant, its value to be dependent on the steady state concentrations of BR, BRI1.BKI1, and BR.BRI1 such that

$$K_d = \frac{r_k^* b^*}{r_b^*}, \quad (20)$$

where K_d denotes the BR.BRI1 dissociation constant, and r_k^* , b^* , and r_b^* denote the steady state concentrations of BRI1.BKI1, BR, and BR.BRI1 respectively. Taking $b^* = [BR]_0$, and rewriting r_k^* , r_b^* in terms of k^* , the steady state concentration of BKI1, (20) may be rewritten as

$$K_d(R_{tot} - K_{tot} + k^*) = (K_{tot} - k^*)[BR]_0. \quad (21)$$

Thus we may solve for k^* to obtain an expression for $[BKI1]_0$:

$$[BKI1]_0 = \frac{K_{tot}[BR]_0 - K_d(R_{tot} - K_{tot})}{K_d + [BR]_0}, \quad (22)$$

and by taking $K_d = 11.2$ nM, the midpoint of values reported in [64], calculate that $[BKI1]_0 = 34.1 \times 10^{-3}$ μ M. Using this value for $[BKI1]_0$ in conjunction with the steady state solution of the second equation in (2), we write

$$\begin{aligned} \beta_k &= \frac{(K_{tot} - [BKI1]_0)[BR]_0}{(R_{tot} - K_{tot} + [BKI1]_0)[BKI1]_0} \beta_b \\ &= 0.329 \beta_b, \end{aligned}$$

giving us an expression for β_k in terms of β_b .

For the second method of calculating $[BKI1]_0$ and β_k , we considered that BRI1 has a state where both BR and BKI1 are bound to it, i.e. the full receptor-based dynamics would look like

$$\begin{aligned} \frac{db}{dt} &= -\beta_1 b r_k + \gamma_1 r_{bk} \\ \frac{dk}{dt} &= -\beta_2 k r_b + \gamma_2 r_{bk} \\ \frac{dr_k}{dt} &= -\beta_1 b r_k + \gamma_1 r_{bk} \\ \frac{dr_b}{dt} &= -\beta_2 k r_b + \gamma_2 r_{bk} \\ \frac{dr_{bk}}{dt} &= \beta_1 b r_k + \beta_2 k r_b - \gamma_1 r_{bk} - \gamma_2 r_{bk} \end{aligned} \quad (23)$$

where the variable r_{bk} denotes the concentration of BR.BRI1.BKI1, and β_1 and β_2 (γ_1 and γ_2) represent the association (dissociation) rates of BR and BRI1.BKI1, and BKI1 and BR.BRI1 (BR.BRI1.BKI1) respectively. Thus the dissociation constant of BR and BRI1.BKI1, and the dissociation constant of BKI1 and BR.BRI1, denoted K_d and K_m respectively, may be defined by

$$K_d = \frac{\gamma_1}{\beta_1}, \quad K_m = \frac{\gamma_2}{\beta_2}.$$

Assuming r_{bk} to be constant allows us to rewrite (23) as

$$\begin{aligned} \frac{db}{dt} &= -\frac{\gamma_2 \beta_1}{\gamma_1 + \gamma_2} b r_k + \frac{\gamma_1 \beta_2}{\gamma_1 + \gamma_2} k r_b, \\ \frac{dk}{dt} &= -\frac{\gamma_1 \beta_2}{\gamma_1 + \gamma_2} k r_b + \frac{\gamma_2 \beta_1}{\gamma_1 + \gamma_2} b r_k, \\ \frac{dr_k}{dt} &= -\frac{\gamma_2 \beta_1}{\gamma_1 + \gamma_2} b r_k + \frac{\gamma_1 \beta_2}{\gamma_1 + \gamma_2} k r_b, \\ \frac{dr_b}{dt} &= -\frac{\gamma_1 \beta_2}{\gamma_1 + \gamma_2} k r_b + \frac{\gamma_2 \beta_1}{\gamma_1 + \gamma_2} b r_k, \end{aligned} \quad (24)$$

which means that we may not only define β_k and β_b as

$$\beta_k = \frac{\gamma_1 \beta_2}{\gamma_1 + \gamma_2}, \quad \beta_b = \frac{\gamma_2 \beta_1}{\gamma_1 + \gamma_2}, \quad (25)$$

but that we may further divide β_k through by β_b to show that

$$\frac{K_d}{K_m} = \frac{\beta_k}{\beta_b},$$

and hence

$$\beta_k = \frac{K_d}{K_m} \beta_b.$$

A value of $K_m = 4.28 \mu\text{M}$ was reported in [61], giving an expression $\beta_k = (2.62 \times 10^{-3}) \beta_b$. The steady state solution of the second equation in (2) may thus be written as

$$(k^*)^2 + \left((R_{tot} - K_{tot}) + \frac{K_m}{K_d} [BR]_0 \right) k^* - \frac{K_m}{K_d} K_{tot} [BR]_0 = 0, \quad (26)$$

which may be solved for k^* , and hence an expression for $[BKI1]_0$ is found

$$\begin{aligned} 0 &= \frac{1}{2} \sqrt{\left((R_{tot} - K_{tot}) + \frac{K_m}{K_d} [BR]_0 \right)^2 + 4 \frac{K_m}{K_d} K_{tot} [BR]_0} \\ &\quad - \frac{1}{2} \left((R_{tot} - K_{tot}) + \frac{K_m}{K_d} [BR]_0 \right), \end{aligned}$$

giving $[BKI1]_0 = 61.3 \times 10^{-3} \mu\text{M}$.

In order to check whether a more accurate estimation of the parameters was given by fitting a non-dimensional model which does not scale time by one of the fitting variables:

$$\begin{aligned} \frac{d\bar{b}}{d\bar{t}} &= \bar{\beta}_k (\kappa - 1 + \bar{k}) \bar{k} - \bar{\beta}_b (1 - \bar{k}) \bar{b} + \bar{\mu}_b \left(\frac{1}{1 + (\bar{\theta}_b \bar{z})^{h_b}} - \bar{b} \right), \\ \epsilon \frac{d\bar{k}}{d\bar{t}} &= \bar{\beta}_b (1 - \bar{k}) \bar{b} - \bar{\beta}_k (\kappa - 1 + \bar{k}) \bar{k}, \\ \frac{d\bar{z}}{d\bar{t}} &= \bar{\delta}_z (1 - \bar{z}) \bar{k} - \bar{\rho}_z \frac{\bar{z}}{1 + (\bar{\theta}_z \bar{z})^{h_z}}, \end{aligned} \quad (27)$$

where

$$\begin{aligned} \bar{\beta}_b &= 60 \beta_b K_{tot}, & \bar{\beta}_k &= 60 \frac{\beta_k (K_{tot})^2 \mu_b}{\alpha_b}, & \kappa &= \frac{R_{tot}}{K_{tot}}, \\ \bar{\mu}_b &= 60 \mu_b, & \bar{\theta}_b &= \theta_b Z_{tot}, & \epsilon &= \frac{K_{tot} \mu_b}{\alpha_b}, \\ \bar{\delta}_z &= 60 \delta_z K_{tot}, & \bar{\rho}_z &= 60 \rho_z, & \bar{\theta}_z &= \theta_z K_{tot}, \end{aligned}$$

(27) was also fitted to the experimental data. The parameters whose dimensional values could be found had close agreement with those found fitting model (2), Tables 4 and 5, and so it is better to consider the fitting of the dimensional model (2) to the experimental data.

B Linearised Stability Analysis for the Model (6) of the BR Signalling Pathway

B.1 Proof of positive invariance of $M = [0, 1 + \beta_k \kappa] \times [0, 1] \times [0, 1]$.

To prove that M is positive invariant, we first consider $M_1 := \{(b, k, z) \in \mathbb{R}^3 \mid b, k, z \geq 0\}$ and show the non-negativity of solutions of (6). Restricting $b = 0$, we obtain that $\mathbf{f} \cdot (1, 0, 0) = \beta_k (\kappa - 1 + k) k + \frac{1}{1 + (\theta_b z)^{h_b}}$, and similarly that $\mathbf{f} \cdot (0, 1, 0) = \frac{\beta_b}{\epsilon} b$ restricting $k = 0$, and $\mathbf{f} \cdot (0, 0, 1) = \delta_z k$ restricting

Constant	Value	Units	Constant	Value	Units
β_b	8.33	$\mu\text{M}^{-1} \text{min}^{-1}$	β_k	2.73	$\mu\text{M}^{-1} \text{min}^{-1}$
α_b	0.27	$\mu\text{M} \text{min}^{-1}$	μ_b	3.58	min^{-1}
δ_z	9.97×10^{-4}	$\mu\text{M}^{-1}\text{min}^{-1}$	ρ_z	1.30×10^{-4}	min^{-1}
θ_z	4.05	μM^{-1}	h_z	6	

Table 4: Transformed parameters when fitting the non-dimensionalised model (27) against experimental data from [50], and using (3) and (4). Due to the nature of the non-dimensionalisation, the dimensional parameters θ_b and Z_{tot} cannot be found.

Constant	Value	Units	Constant	Value	Units
β_b	8.06	$\mu\text{M}^{-1} \text{min}^{-1}$	β_k	2.11×10^{-2}	$\mu\text{M}^{-1} \text{min}^{-1}$
α_b	0.27	$\mu\text{M} \text{min}^{-1}$	μ_b	3.68	min^{-1}
δ_z	1.77×10^{-3}	$\mu\text{M}^{-1}\text{min}^{-1}$	ρ_z	4.33×10^{-4}	min^{-1}
θ_z	3.98	μM^{-1}	h_z	6	

Table 5: Transformed parameters when fitting the non-dimensionalised model (27) against experimental data from [50], and using (3) and (5). Due to the nature of the non-dimensionalisation, the dimensional parameters θ_b and Z_{tot} cannot be found.

	WT1	BRZ1	WT2	BL2	MUT3	BRZ3	MUT4	BL4
β_b	8.33	8.49	8.50	8.42	2.36×10^{-3}	2.46×10^{-3}	2.43×10^{-3}	2.31×10^{-3}
β_k	2.73	2.72	2.72	2.80	3.26×10^{-12}	3.10×10^{-12}	2.95×10^{-12}	3.09×10^{-12}
α_b	0.27	6.29×10^{-2}	6.29×10^{-2}	6.08×10^{-2}	0.27	0.27	0.28	0.27
θ_b	1.96	2.01	2.01	2.11	1.96	1.96	1.92	1.88
μ_b	3.58	3.54	3.54	13.98	3.50	3.40	3.40	3.57
δ_z	1.02×10^{-3}	1.05×10^{-3}	1.07×10^{-3}	1.10×10^{-3}	1.02×10^{-3}	1.01×10^{-3}	1.01×10^{-3}	1.06×10^{-3}
Z_{tot}	2.65	2.72	2.72	2.75	2.65	2.58	2.58	2.58
ρ_z	1.33×10^{-4}	1.39×10^{-4}	1.32×10^{-4}	1.32×10^{-4}	1.34×10^{-4}	1.33×10^{-4}	1.29×10^{-4}	1.22×10^{-4}
θ_z	3.95	4.10	4.30	4.06	3.76	3.93	3.91	3.91
h_z	6.02	5.82	5.52	5.65	5.95	5.75	5.76	5.76

Table 6: Fitted model parameters obtained by fitting model (2) under conditions (4),(3) to experimental data for each growth condition. Here WT1 corresponds to the case where wild-type plants were grown under control conditions, BZR1 to the case where wild-type plants were grown in a medium containing BRZ, WT2 to the case where wild-type plants had been grown in a medium containing BRZ $5\mu\text{M}$ for two days, BL2 to the case where wild-type plants had been grown in a medium containing BRZ $5\mu\text{M}$ for two days and then supplemented with $0.1\mu\text{M}$ BL, MUT3 corresponds to the case where mutant plants were grown under control conditions, BZR4 to the case where mutant plants were grown in a medium containing BRZ, MUT4 to the case where mutant plants had been grown in a medium containing BRZ $5\mu\text{M}$ for two days, BL4 to the case where mutant plants had been grown in a medium containing BRZ $5\mu\text{M}$ for two days and then supplemented with $0.1\mu\text{M}$ BL.

$z = 0$. Since $b, k, z \geq 0$ we also obtain that $\mathbf{f}(u) \cdot \mathbf{n}(u) \geq 0 \forall u \in \partial M_1$ and any flow that starts in M_1 must remain in M_1 for all t , and hence M_1 is a positive invariant set. To show boundedness of solutions of (6), consider $M_2 := \{(b, k, z) \in \mathbb{R}^3 \mid b \leq 1 + \beta_k \kappa, k \leq 1, z \leq 1\}$. Restricting $b = 1 + \beta_k \kappa$, we obtain that $\mathbf{f} \cdot (-1, 0, 0) = (\beta_b(1 - k) + 1)(1 + \beta_k \kappa) - \beta_k(\kappa - 1 + k)k - \frac{1}{1 + (\theta_b z)^{h_b}}$, and similarly that $\mathbf{f} \cdot (0, -1, 0) = \frac{\beta_k}{\epsilon} \kappa$ restricting $k = 1$, and $\mathbf{f} \cdot (0, 0, -1) = \frac{\rho_z}{1 + (\theta_z k)^{h_z}}$ restricting $z = 1$. Note that $\mathbf{f} \cdot (-1, 0, 0)$ has no critical points for $0 \leq k \leq 1$, and has value $\beta_b(1 + \beta_k \kappa)$ for $k = 0$, and 0 for $k = 1$. Thus $\mathbf{f}(u) \cdot \mathbf{n}(u) \geq 0 \forall (u) \in \partial M_2$ and any flow that starts in M_2 must remain in M_2 for all t , hence M_2 is a positive invariant set. Thus $M := M_1 \cap M_2$ is a positive invariant region [5].

B.2 Calculations for the proof of Theorem 2

Any steady state (b^*, k^*, z^*) of (6) satisfies

$$\begin{aligned} 0 &= \frac{1}{1 + (\theta_b z^*)^{h_b}} - b^*, \\ 0 &= \beta_b(1 - k^*)b^* - \beta_k(\kappa - 1 + k^*)k^*, \\ 0 &= -\rho_z \frac{z^*}{1 + (\theta_z k^*)^{h_z}} + \delta_z(1 - z^*)k^*. \end{aligned}$$

Using simple algebraic manipulation on the system above, we find b^* and z^* in terms of k^*

$$\begin{aligned} b^* &= \frac{1}{1 + \left(\theta_b \frac{\delta_z k^* (1 + (\theta_z k^*)^{h_z})}{\rho_z + \delta_z k^* (1 + (\theta_z k^*)^{h_z})} \right)^{h_b}} = \frac{\beta_k (\kappa - 1 + k^*) k^*}{\beta_b (1 - k^*)}, \\ z^* &= \frac{\delta_z k^* (1 + (\theta_z k^*)^{h_z})}{\rho_z + \delta_z k^* (1 + (\theta_z k^*)^{h_z})}. \end{aligned}$$

Then k^* is defined as a root of the following non-linear function

$$\begin{aligned} g(k^*) &:= \beta_k (\kappa - 1 + k^*) k^* \left(1 + \left(\frac{\theta_b \delta_z k^* (1 + (\theta_z k^*)^{h_z})}{\rho_z + \delta_z k^* (1 + (\theta_z k^*)^{h_z})} \right)^{h_b} \right) \\ &\quad - \beta_b (1 - k^*). \end{aligned}$$

The derivative of g

$$\begin{aligned} \frac{dg}{dk^*} &= \beta_b + \beta_k(\kappa - 1 + 2k^*) \left(1 + \left(\theta_b \frac{\delta_z k^* (1 + (\theta_z k^*)^{h_z})}{\rho_z + \delta_z k^* (1 + (\theta_z k^*)^{h_z})} \right)^{h_b} \right) \\ &\quad + \beta_k(\kappa - 1 + k^*)k^* \times \\ &\quad \times \left(\frac{h_b \theta_b \delta_z \rho_z (1 + (1 + h_z)(\theta_z k^*)^{h_z})}{(\rho_z + \delta_z k^* (1 + (\theta_z k^*)^{h_z}))^2} \left(\frac{\theta_b \delta_z k^* (1 + (\theta_z k^*)^{h_z})}{\rho_z + \delta_z k^* (1 + (\theta_z k^*)^{h_z})} \right)^{h_b - 1} \right) \end{aligned}$$

which is positive for all $p \in P$ and $k^* \in [0, 1]$.

B.3 Characteristic Equation

The Jacobian for system (6) evaluated at the steady state (b^*, k^*, z^*) is given by

$$\begin{pmatrix} -\beta_b(1 - k^*) - 1 & \beta_k(\kappa - 1 + 2k^*) + \beta_b b^* & -\frac{h_b \theta_b (\theta_b z^*)^{h_b - 1}}{(1 + (\theta_b z^*)^{h_b})^2} \\ \frac{\beta_b(1 - k^*)}{\epsilon} & -\frac{\beta_b b^*}{\epsilon} - \frac{\beta_k(\kappa - 1 + 2k^*)}{\epsilon} & 0 \\ 0 & \delta_z(1 - z^*) + \frac{\rho_z h_z \theta_z z^{*h_z - 1}}{(1 + (\theta_z k^*)^{h_z})^2} & -\delta_z k^* - \frac{\rho_z}{1 + (\theta_z k^*)^{h_z}} \end{pmatrix} \quad (28)$$

The coefficients of the characteristic equation associated to Jacobian J (28) are defined as follows

$$\begin{aligned} a_2 &= \beta_b(1 - k^*) + 1 + \frac{\beta_b b^*}{\epsilon} + \frac{\beta_b}{\epsilon}(\kappa - 1 + 2k^*) + \delta_z k^* + \frac{\rho_z}{1 + (\theta_z k^*)^{h_z}}, \\ a_1 &= \frac{1}{\epsilon} (\beta_b b^* + \beta_k(\kappa - 1 + 2k^*)) \left(\beta_b(1 - k^*) + 2 + \delta_z k^* + \frac{\rho_z}{1 + (\theta_z k^*)^{h_z}} \right) \\ &\quad + (\beta_b(1 - k^*) + 1) \left(\delta_z k^* + \frac{\rho_z}{1 + (\theta_z k^*)^{h_z}} \right), \\ a_0 &= \frac{1}{\epsilon} \beta_b(1 - k^*) \frac{\theta_b h_b (\theta_b z^*)^{h_b - 1}}{(1 + (\theta_b z^*)^{h_b})^2} \left(\delta_z(1 - z^*) + \frac{\rho_z z^* \theta_z h_z (\theta_z k^*)^{h_z - 1}}{(1 + (\theta_z k^*)^{h_z})^2} \right) \\ &\quad + \frac{1}{\epsilon} (\beta_b b^* + \beta_k(\kappa - 1 + 2k^*)) \left(\delta_z k^* + \frac{\rho_z}{1 + (\theta_z k^*)^{h_z}} \right), \end{aligned}$$

where (b^*, k^*, z^*) is a steady state of the system (6).

C Non-dimensionalisation of Model (7)-(9) of the BR Signalling Pathway

Since in the PDE-ODE model (7)-(9) some of the variables are defined on the boundaries we must consider them in units of mol/m^2 instead of mol/m^3 , compared to the ODE model (2). To adapt the units, we scale by the length of the cell segment, i.e. $\tilde{r}_k = l_c r_k$, $\tilde{r}_b = l_c r_b$ and $\tilde{z} = l_c z$. To preserve the balance of units in the system, we must scale the following parameters $\tilde{\alpha}_b = l_c \alpha_b$, $\tilde{\theta}_b = \theta_b/l_c$, $\tilde{\delta}_z = l_c \delta_z$. Applying this scaling and non-dimensionalising via $t = t^* \bar{t}$, $x = l_c y$, $b = b^* \bar{b}$, $k = k^* \bar{k}$, $\tilde{r}_k = r_k^* \bar{r}_k$, $\tilde{r}_b = r_b^* \bar{r}_b$, $\tilde{z} = z^* \bar{z}$, $z_p = z_p^* \bar{z}_p$, system (7)-(9) is transformed to

$$\left. \begin{aligned} \partial_{\bar{t}} \bar{b} &= \frac{D_b t^*}{(x^*)^2} \partial_y^2 \bar{b} - \mu_b t^* \bar{b} \\ \partial_{\bar{t}} \bar{k} &= \frac{D_k t^*}{(x^*)^2} \partial_y^2 \bar{k} \\ \partial_{\bar{t}} \bar{z}_p &= \frac{D_z t^*}{(x^*)^2} \partial_y^2 \bar{z}_p \end{aligned} \right\} \text{in } \bar{\Omega}_c, \quad (29)$$

$$\left. \begin{aligned} -\frac{D_b t^*}{(x^*)^2} \partial_y \bar{b} &= \frac{\beta_k t^* r_b^* k^*}{x^* b^*} \bar{r}_b \bar{k} - \frac{\beta_b t^* r_k^*}{x^*} \bar{b} \bar{r}_k \\ -\frac{D_k t^*}{(x^*)^2} \partial_y \bar{k} &= \frac{\beta_b t^* r_k^* b^*}{x^* k^*} \bar{b} \bar{r}_k - \frac{\beta_k t^* r_b^*}{x^*} \bar{r}_b \bar{k} \\ \frac{d\bar{r}_k}{d\bar{t}} &= \beta_k k^* t^* \bar{r}_b \bar{k} - \beta_b b^* t^* \bar{b} \bar{r}_k \\ \frac{d\bar{r}_b}{d\bar{t}} &= \beta_b b^* t^* \bar{b} \bar{r}_k - \beta_k k^* t^* \bar{r}_b \bar{k} \\ -\frac{D_z t^*}{(x^*)^2} \partial_y \bar{z}_p &= 0 \end{aligned} \right\} \text{on } \bar{\Gamma}_c, \quad (30)$$

$$\left. \begin{aligned} \frac{D_b t^*}{(x^*)^2} \partial_y \bar{b} &= \frac{l_c \alpha_b t^*}{x^* b^* (1 + (\frac{\theta_b z^* \bar{z}}{l_c})^{h_b})} \\ \frac{D_k t^*}{(x^*)^2} \partial_y \bar{k} &= 0 \\ \frac{d\bar{z}}{d\bar{t}} &= \frac{l_c \delta_z t^* p^* k^*}{z^*} \bar{z}_p \bar{k} - \rho_z t^* \frac{\bar{z}}{1 + (\theta_z k^* \bar{k})^{h_z}} \\ \frac{D_z t^*}{(x^*)^2} \partial_y \bar{z}_p &= -\frac{l_c \delta_z t^* k^*}{x^*} \bar{z}_p \bar{k} + \frac{\rho_z t^* z^*}{x^* p^*} \frac{\bar{z}}{1 + (\theta_z k^* \bar{k})^{h_z}} \end{aligned} \right\} \text{on } \bar{\Gamma}_n. \quad (31)$$

Take $t^* = 1/\mu_b$, $x^* = l_c$, $b^* = \alpha_b/\mu_b$, $k^* = K_{tot}$, $r_k^* = l_c R_{tot}$, $r_b^* = l_c R_{tot}$, $z^* = l_c Z_{tot}$ and $p^* = Z_{tot}$. Then

$$\left. \begin{aligned} \partial_{\bar{t}} \bar{b} &= \bar{D}_b \partial_y^2 \bar{b} - \bar{b} \\ \partial_{\bar{t}} \bar{k} &= \bar{D}_k \partial_y^2 \bar{k} \\ \partial_{\bar{t}} \bar{z}_p &= \bar{D}_z \partial_y^2 \bar{z}_p \end{aligned} \right\} \text{in } \bar{\Omega}_c. \quad (32)$$

$$\left. \begin{aligned} -\bar{D}_b \partial_y \bar{b} &= \bar{\beta}_k \bar{r}_b \bar{k} - \bar{\beta}_b \bar{b} \bar{r}_k \\ -\bar{D}_k \partial_y \bar{k} &= \epsilon_1 (\bar{\beta}_b \bar{r}_k \bar{b} - \bar{\beta}_k \bar{r}_b \bar{k}) \\ \frac{d\bar{r}_k}{d\bar{t}} &= \epsilon_2 (\bar{\beta}_k \bar{r}_b \bar{k} - \bar{\beta}_b \bar{b} \bar{r}_k) \\ \frac{d\bar{r}_b}{d\bar{t}} &= \epsilon_2 (\bar{\beta}_b \bar{b} \bar{r}_k - \bar{\beta}_k k^* t^* \bar{r}_b \bar{k}) \\ -\bar{D}_z \partial_y \bar{z}_p &= 0 \end{aligned} \right\} \text{on } \bar{\Gamma}_c, \quad (33)$$

$$\left. \begin{aligned}
\bar{D}_b \partial_y \bar{b} &= \frac{1}{1 + (\bar{\theta}_b \bar{z})^{h_b}} \\
\bar{D}_k \partial_y \bar{k} &= 0 \\
\frac{d\bar{z}}{d\bar{t}} &= \bar{\delta}_z \bar{z}_p \bar{k} - \bar{\rho}_z \frac{\bar{z}}{1 + (\bar{\theta}_z \bar{k})^{h_z}} \\
\bar{D}_z \partial_y \bar{z}_p &= -\bar{\delta}_z \bar{z}_p \bar{k} + \bar{\rho}_z \frac{\bar{z}}{1 + (\bar{\theta}_z \bar{k})^{h_z}}
\end{aligned} \right\} \text{on } \bar{\Gamma}_n, \quad (34)$$

where

$$\begin{aligned}
\bar{D}_b &= \frac{D_b}{\mu_b l_c^2}, & \bar{D}_k &= \frac{D_k}{\mu_b l_c^2}, & \bar{D}_z &= \frac{D_z}{\mu_b l_c^2}, & \bar{\beta}_k &= \frac{\beta_k R_{tot} K_{tot}}{\alpha_b}, \\
\bar{\beta}_b &= \frac{\beta_b R_{tot}}{\beta_b R_{tot}}, & \epsilon_1 &= \frac{\alpha_b}{K_{tot} \mu_b}, & \epsilon_2 &= \frac{\alpha_b}{R_{tot} \mu_b}, & \bar{\theta}_b &= \theta_b Z_{tot}, \\
\bar{\delta}_z &= \frac{\delta_z K_{tot}}{\mu_b}, & \bar{\rho}_z &= \frac{\rho_z}{\mu_b}, & \bar{\theta}_z &= \theta_z K_{tot}.
\end{aligned}$$

D Rigorous Reduction of the Model for GA Signalling Pathway from [36]

Here we present the rigorous reduction of the model for the GA signalling pathway from [36] to the system of ODEs (10) and (11) for GA, GID1, DELLA, GA.GID1^o, GA.GID1^c, DELLA.GA.GID1^c, GID1_m and DELLA_m. To do this we assume that the dynamics of the actual biosynthesis may be captured from the DELLA dynamics only. We also assume only one functional form of the DELLA.GID1.GA complex. To save space we denote the independent variables by x_i for $i = 1, \dots, 21$, in the same order as the full statement of the model in [36].

To describe GA signal transduction:

$$\frac{dx_1}{dt} = -l_a x_1 x_{11} + l_d x_2 + \delta_{gid1} x_{20} - \mu_{gid1} x_1, \quad (35a)$$

$$\frac{dx_2}{dt} = l_a x_1 x_{11} - l_d x_2 + p x_3 - q x_2, \quad (35b)$$

$$\frac{dx_3}{dt} = -p x_3 + q x_2 - (u_{a1} + u_{a2}) x_6 x_3 + (u_{d1} + u_m) x_4 + u_{d2} x_5, \quad (35c)$$

$$\frac{dx_4}{dt} = u_{a1} x_6 x_3 - (u_{d1} + u_m) x_4, \quad (35d)$$

$$\frac{dx_5}{dt} = u_{a2} x_6 x_3 - u_{d2} x_5, \quad (35e)$$

$$\frac{dx_6}{dt} = -(u_{a1} + u_{a2}) x_6 x_3 + u_{d1} x_4 + u_{d2} x_5 + \delta_{della} x_{21}. \quad (35f)$$

To describe GA biosynthesis:

$$\frac{dx_7}{dt} = \omega_{ga12} - k_{a12} x_7 x_{16} + k_{d12} x_{12} - \mu_{ga} x_7, \quad (36a)$$

$$\frac{dx_8}{dt} = -k_{a15} x_8 x_{16} + k_{d15} x_{13} + k_{m12} x_{12} - \mu_{ga} x_8, \quad (36b)$$

$$\frac{dx_9}{dt} = -k_{a24} x_9 x_{16} + k_{d24} x_{14} + k_{m15} x_{13} - \mu_{g1} x_9, \quad (36c)$$

$$\frac{dx_{10}}{dt} = -k_{a9} x_{10} x_{17} + k_{d9} x_{15} + k_{m24} x_{14} - \mu_{ga} x_{10}, \quad (36d)$$

$$\begin{aligned} \frac{dx_{11}}{dt} &= P_{mem} \frac{S_{root}}{R_{root}} (A_1 \omega_{ga4} - B_1 x_{11}) + k_{m9} x_{15} - l_a x_1 x_{11} + l_d x_2 \\ &\quad - \mu_{ga} x_{11}. \end{aligned} \quad (36e)$$

To describe complexes of GAs and enzymes:

$$\frac{dx_{12}}{dt} = k_{a12}x_7x_{16} - (k_{d12} + k_{m12})x_{12}, \quad (37a)$$

$$\frac{dx_{13}}{dt} = k_{a15}x_8x_{16} - (k_{d15} + k_{m15})x_{13}, \quad (37b)$$

$$\frac{dx_{14}}{dt} = k_{a24}x_9x_{16} - (k_{d24} + k_{m24})x_{14}, \quad (37c)$$

$$\frac{dx_{15}}{dt} = k_{a9}x_{10}x_{17} - (k_{d9} + k_{m9})x_{15}. \quad (37d)$$

To describe the enzymes:

$$\begin{aligned} \frac{dx_{16}}{dt} = & -k_{a12}x_7x_{16} - k_{a15}x_8x_{16} - k_{a24}x_9x_{16} + (k_{d12} + k_{m12})x_{12} \\ & + (k_{d15} + k_{m15})x_{13} + (k_{d24} + k_{m24})x_{14} + \delta_{ga20ox}x_{18} \\ & - \mu_{ga20ox}x_{16}, \end{aligned} \quad (38a)$$

$$\frac{dx_{17}}{dt} = -k_{a9}x_{10}x_{17} + (k_{d9} + k_{m9})x_{15} + \delta_{ga3ox}x_{19} - \mu_{ga3ox}x_{17}. \quad (38b)$$

To describe the mRNAs:

$$\frac{dx_{18}}{dt} = \phi_{ga20ox} \left(\frac{x_6}{x_6 + \theta_{ga20ox}} - x_{18} \right), \quad (39a)$$

$$\frac{dx_{19}}{dt} = \phi_{ga3ox} \left(\frac{x_6}{x_6 + \theta_{ga3ox}} - x_{19} \right), \quad (39b)$$

$$\frac{dx_{20}}{dt} = \phi_{gid1} \left(\frac{x_6}{x_6 + \theta_{gid1}} - x_{20} \right), \quad (39c)$$

$$\frac{dx_{21}}{dt} = \phi_{della} \left(\frac{\theta_{della}}{x_6 + \theta_{della}} - x_{21} \right). \quad (39d)$$

We set Eq (35e) to zero since we assume that only one configuration of the DELLA.GID1^c.GA₄ can form. Since the conversion of GA₄ precursors occurs on a relatively fast scale we set the time-derivatives in (36a)-(36d) and (37a)-(39b) equal to zero. We immediately remove 3 variables by noting from Eqs. (35e), (39a) and (39b) that

$$x_5 = \frac{u_{a2}}{u_{d2}}x_6x_3, \quad (40a)$$

$$x_{18} = \frac{x_6}{x_6 + \theta_{ga20ox}}, \quad (40b)$$

$$x_{19} = \frac{x_6}{x_6 + \theta_{ga3ox}}, \quad (40c)$$

and further from Eqs. (36a)-(36d), and (37a)-(38b) that

$$x_{16} = \frac{\delta_{ga20ox}}{\mu_{ga20ox}} \frac{x_6}{x_6 + \theta_{ga20ox}}, \quad (41a)$$

$$x_{17} = \frac{\delta_{ga3ox}}{\mu_{ga3ox}} \frac{x_6}{x_6 + \theta_{ga3ox}}, \quad (41b)$$

$$k_{m9}x_{15} = \omega_{ga12} - \mu_{ga}(x_7 + x_8 + x_9 + x_{10}), \quad (41c)$$

with

$$x_7 = \frac{\omega_{ga12}}{\mu_{ga} + K_{12}}, \quad (42a)$$

$$x_8 = \frac{\omega_{ga12}K_{12}}{(\mu_{ga} + K_{12})(\mu_{ga} + K_{15})}, \quad (42b)$$

$$x_9 = \frac{\omega_{ga12}K_{12}K_{15}}{(\mu_{ga} + K_{12})(\mu_{ga} + K_{15})(\mu_{ga} + K_{24})}, \quad (42c)$$

$$x_{10} = \frac{\omega_{ga12}K_{12}K_{15}K_{24}}{(\mu_{ga} + K_{12})(\mu_{ga} + K_{15})(\mu_{ga} + K_{24})(\mu_{ga} + K_9)}, \quad (42d)$$

where

$$\begin{aligned}
K_{12} &= \frac{\delta_{ga20ox} k_{a12} k_{m12}}{\mu_{ga20ox} (k_{d12} + k_{m12})} \frac{x_6}{x_6 + \theta_{ga20ox}}, \\
K_{15} &= \frac{\delta_{ga20ox} k_{a15} k_{m15}}{\mu_{ga20ox} (k_{d15} + k_{m15})} \frac{x_6}{x_6 + \theta_{ga20ox}}, \\
K_{24} &= \frac{\delta_{ga20ox} k_{a24} k_{m24}}{\mu_{ga20ox} (k_{d24} + k_{m24})} \frac{x_6}{x_6 + \theta_{ga20ox}}, \\
K_9 &= \frac{\delta_{ga3ox} k_{a9} k_{m9}}{\mu_{ga3ox} (k_{d9} + k_{m9})} \frac{x_6}{x_6 + \theta_{ga3ox}}.
\end{aligned}$$

Substituting these into Eq.(41c)

$$\begin{aligned}
k_{m9}x_{15} &= \omega_{ga12} \left\langle 1 - \mu_{ga} \left[\frac{\begin{pmatrix} (\mu_{ga} + K_{15})(\mu_{ga} + K_{24})(\mu_{ga} + K_9) \\ + K_{12}(\mu_{ga} + K_{24})(\mu_{ga} + K_9) \\ + K_{12}K_{15}(\mu_{ga} + K_9) + K_{12}K_{15}K_{24} \end{pmatrix}}{(\mu_{ga} + K_{12})(\mu_{ga} + K_{15})(\mu_{ga} + K_{24})(\mu_{ga} + K_9)} \right] \right\rangle \\
&= \omega_{ga12} \frac{K_{12}K_{15}K_{24}K_9}{(\mu_{ga} + K_{12})(\mu_{ga} + K_{15})(\mu_{ga} + K_{24})(\mu_{ga} + K_9)},
\end{aligned}$$

which can be multiplied through by the Hill function denominators, and upon simplifying to fourth order terms in x_6 becomes

$$k_{m9}x_{15} = \alpha_g \frac{x_6^4}{x_6^4 + \theta_{ga}},$$

where

$$\alpha_g = \frac{\omega_{ga12} \delta_{ga3ox} (\delta_{ga20ox})^3 k_{a12} k_{m12} k_{a15} k_{m15} k_{a24} k_{m24} k_{a9} k_{m9}}{\begin{pmatrix} (\mu_{ga} \mu_{ga20ox} (k_{d12} + k_{m12}) + \delta_{ga20ox} k_{a12} k_{m12}) \times \\ \times (\mu_{ga} \mu_{ga20ox} (k_{d15} + k_{m15}) + \delta_{ga20ox} k_{a15} k_{m15}) \times \\ \times (\mu_{ga} \mu_{ga20ox} (k_{d24} + k_{m24}) + \delta_{ga20ox} k_{a24} k_{m24}) \times \\ \times (\mu_{ga} \mu_{ga3ox} (k_{d9} + k_{m9}) + \delta_{ga3ox} k_{a9} k_{m9}) \end{pmatrix}}$$

and

$$\theta_{ga} = \frac{\begin{pmatrix} \mu_{ga}^4 \theta_{ga3ox} (\theta_{ga20ox})^3 \mu_{ga3ox} (\mu_{ga20ox})^3 (k_{d12} + k_{m12}) * \\ *(k_{d15} + k_{m15})(k_{d24} + k_{m24})(k_{d9} + k_{m9}) \end{pmatrix}}{\begin{pmatrix} (\mu_{ga} \mu_{ga20ox} (k_{d12} + k_{m12}) + \delta_{ga20ox} k_{a12} k_{m12}) \times \\ \times (\mu_{ga} \mu_{ga20ox} (k_{d15} + k_{m15}) + \delta_{ga20ox} k_{a15} k_{m15}) \times \\ \times (\mu_{ga} \mu_{ga20ox} (k_{d24} + k_{m24}) + \delta_{ga20ox} k_{a24} k_{m24}) \times \\ \times (\mu_{ga} \mu_{ga3ox} (k_{d9} + k_{m9}) + \delta_{ga3ox} k_{a9} k_{m9}) \end{pmatrix}}.$$

Thus, we obtain a reduced model that reads

$$\frac{dx_1}{dt} = -l_a x_1 x_{11} + l_d x_2 + \delta_{gid1} x_{20} - \mu_{gid1} x_1, \quad (43a)$$

$$\frac{dx_2}{dt} = l_a x_1 x_{11} - l_d x_2 + p x_3 - q x_2, \quad (43b)$$

$$\frac{dx_3}{dt} = -p x_3 + q x_2 - (u_{a1} + u_{a2}) x_6 x_3 + (u_{d1} + u_m) x_4, \quad (43c)$$

$$\frac{dx_4}{dt} = u_{a1} x_6 x_3 - (u_{d1} + u_m) x_4, \quad (43d)$$

$$\frac{dx_6}{dt} = -u_{a1} x_6 x_3 + u_{d1} x_4 + \delta_{della} x_{21}, \quad (43e)$$

$$\begin{aligned}
\frac{dx_{11}}{dt} &= P_{mem} \frac{S_{root}}{R_{root}} (A_1 \omega_{ga4} - B_1 x_{11}) + \alpha_g \frac{x_6^4}{x_6^4 + \theta_{ga}} - l_a x_1 x_{11} \\
&\quad + l_d x_2 - \mu_{ga} x_{11},
\end{aligned} \quad (43f)$$

$$\frac{dx_{20}}{dt} = \phi_{gid1} \left(\frac{x_6}{x_6 + \theta_{gid1}} - x_{20} \right), \quad (43g)$$

$$\frac{dx_{21}}{dt} = \phi_{della} \left(\frac{\theta_{della}}{x_6 + \theta_{della}} - x_{21} \right). \quad (43h)$$

E Non-dimensionalisation of the model including spatial heterogeneity in the crosstalk signalling

Again applying scaling and non-dimensionalising via $t = t^* \bar{t}$ etc, system (15)-(19) transforms into

$$\left. \begin{aligned} \partial_{\bar{t}} \bar{b} &= \frac{D_b t^*}{(x^*)^2} \partial_y^2 \bar{b} - \mu_b t^* \bar{b} \\ \partial_{\bar{t}} \bar{k} &= \frac{D_k t^*}{(x^*)^2} \partial_y^2 \bar{k} \\ \partial_{\bar{t}} \bar{z}_p &= \frac{D_z t^*}{(x^*)^2} \partial_y^2 \bar{z}_p \\ \partial_{\bar{t}} \bar{g} &= \frac{D_g t^*}{(x^*)^2} \partial_y^2 \bar{g} - \mu_g t^* \bar{g} \end{aligned} \right\} \text{in } \bar{\Omega}_c,$$

and receptor based interactions of BR, BKI1 and BRI1 and influx of exogenous GA occur on the plasma membrane

$$\left. \begin{aligned} -\frac{D_b t^*}{(x^*)^2} \partial_y \bar{b} &= \frac{\beta_k t^* r_b^* k^*}{x^* b^*} \bar{r}_b \bar{k} - \frac{\beta_b t^* r_k^*}{x^*} \bar{r}_k \bar{b} \\ -\frac{D_k t^*}{(x^*)^2} \partial_y \bar{k} &= \frac{\beta_b t^* r_k^* b^*}{x^* k^*} \bar{r}_k \bar{b} - \frac{\beta_k t^* r_b^*}{x^*} \bar{r}_b \bar{k} \\ -\frac{D_z t^*}{(x^*)^2} \partial_y \bar{z}_p &= 0 \\ -\frac{D_g t^*}{(x^*)^2} \partial_y \bar{g} &= 0 \\ \frac{d\bar{r}_k}{d\bar{t}} &= \frac{\beta_k r_b^* k^* t^*}{r_k^*} \bar{r}_b \bar{k} - \beta_b b^* t^* \bar{r}_k \bar{b} \\ \frac{d\bar{r}_b}{d\bar{t}} &= \frac{\beta_b r_k^* b^* t^*}{r_b^*} \bar{r}_k \bar{b} - \beta_k k^* t^* \bar{r}_b \bar{k} \end{aligned} \right\} \text{on } \bar{\Gamma}_c.$$

We assume that production of BR, change in phosphorylation status of BZR and interactions between BZR and DELLA occur in the nucleus

$$\left. \begin{aligned} \frac{D_b t^*}{(x^*)^2} \partial_y \bar{b} &= \frac{l_c \alpha_b t^*}{1 + \left(\frac{\theta_b z^* \bar{z}}{l_c}\right)^{h_b}} \\ \frac{D_k t^*}{(x^*)^2} \partial_y \bar{k} &= 0 \\ \frac{d\bar{z}}{d\bar{t}} &= \frac{l_c \delta_z t^* z_p^* k^*}{z^*} \bar{z}_p \bar{k} - \rho_z t^* \frac{\bar{z}}{1 + (\theta_z k^* \bar{k})^{h_z}} - \frac{\beta_z t^*}{l_c} \bar{z} \bar{d}_l + \frac{\gamma_z z_d^* t^*}{z^*} \bar{z}_d \\ \frac{D_z t^*}{(x^*)^2} \partial_y \bar{z}_p &= -\frac{l_c \delta_z t^* k^*}{x^*} \bar{z}_p \bar{k} + \frac{\rho_z z^* t^*}{x^* z_p^*} \frac{\bar{z}}{1 + (\theta_z k^* \bar{k})^{h_z}} \end{aligned} \right\} \text{on } \bar{\Gamma}_n.$$

We assume all constituent processes of the GA signalling pathway apart from degradation and influx of GA also occur in the nucleus

$$\left. \begin{aligned}
\frac{d\bar{r}}{dt} &= -\beta_g t^* g^* \bar{r} \bar{g} + \frac{\gamma_g r_g^{o*} t^*}{r^*} \bar{r}_g^o + \frac{l_c \alpha_r t^*}{r^*} \bar{r}_m - \mu_r t^* \bar{r} \\
\frac{d\bar{r}_g^o}{dt} &= \frac{\beta_g r^* g^*}{r_g^{o*}} \bar{r} \bar{g} - (\gamma_g + \lambda^c) t^* \bar{r}_g^o + \frac{\lambda^o r_g^{c*} t^*}{r_g^{o*}} \bar{r}_g^c \\
\frac{d\bar{r}_g^c}{dt} &= \frac{\lambda^c r_g^{o*} t^*}{r_g^{c*}} \bar{r}_g^o - \lambda^o t^* \bar{r}_g^c - \frac{\beta_d d_l^* t^*}{l_c} \bar{d}_l \bar{r}_g^c + \frac{(\gamma_d + \mu_d) r_d^* t^*}{r_g^{c*}} \bar{r}_d \\
\frac{d\bar{r}_d}{dt} &= \frac{\beta_d d_l^* r_g^{c*} t^*}{l_c r_d^*} \bar{d}_l \bar{r}_g^c - (\gamma_d + \mu_d) t^* \bar{r}_d \\
\frac{d\bar{d}_l}{dt} &= -\frac{\beta_d r_g^{c*} t^*}{l_c} \bar{d}_l \bar{r}_g^c + \frac{\gamma_d r_d^* t^*}{d_l^*} \bar{r}_d + \frac{l_c \alpha_d t^*}{d_l^*} \bar{d}_m - \beta_z z^* t^* \bar{z} \bar{d}_l + \frac{\gamma_z z_d^*}{d_l^*} \bar{z}_d \\
\frac{D_g t^*}{(x^*)^2} \partial_y \bar{g} &= \frac{l_c \alpha_g t^*}{x^* g^*} \frac{\left(\bar{d}_l + \frac{\phi_z z^*}{d_l^*} \bar{z}\right)^4}{\left(\frac{l_c \vartheta_g}{(d_l^*)^4} + \left(\bar{d}_l + \frac{\phi_z z^*}{d_l^*} \bar{z}\right)^4\right)} - \frac{\beta_g r^* t^*}{x^*} \bar{r} \bar{g} + \frac{\gamma_g r_g^{o*}}{x^* g^*} \bar{r}_g^o \\
\frac{d\bar{r}_m}{dt} &= \phi_r t^* \left(\frac{\bar{d}_l}{\frac{l_c \theta_r}{d_l^*} + \bar{d}_l} - \bar{r}_m \right) \\
\frac{d\bar{d}_m}{dt} &= \phi_d t^* \left(\frac{\frac{\theta_d}{d_l^*}}{\frac{\theta_d}{d_l^*} + \bar{d}_l} - \bar{d}_m \right)
\end{aligned} \right\} \text{ on } \Gamma_n.$$

Finally we assume cross-talk via formation of the BZR.DELLA complex also occurs in the nucleus

$$\frac{d\bar{z}_d}{dt} = \frac{\beta_z z^* d_l^*}{z_d^*} \bar{z} \bar{d}_l - \gamma_z t^* \bar{z}_d \quad \text{on } \Gamma_n.$$

We set

$$\begin{aligned}
t^* &= \frac{1}{\gamma_z}, & x^* &= l_c, & b^* &= \frac{\alpha_b}{\mu_b}, & k^* &= K_{tot}, & r_k^* &= l_c R_{tot}, \\
r_b^* &= l_c R_{tot}, & z^* &= l_c Z_{tot}, & z_p^* &= Z_{tot}, & r^* &= \frac{l_c \alpha_r}{\mu_r}, & r_g^{o*} &= \frac{l_c \alpha_r}{\mu_r}, \\
r_g^{c*} &= \frac{l_c \alpha_r}{\mu_r}, & r_d^* &= \frac{l_c \alpha_r}{\mu_r}, & d_l^* &= \frac{l_c \alpha_d}{\mu_d}, & g^* &= \frac{\alpha_g}{\mu_g}, & z_d^* &= l_c Z_{tot},
\end{aligned}$$

and introduce the new dimensionless parameters

$$\begin{aligned}
\bar{D}_b &= \frac{D_b}{\gamma_c l_c^2}, & \bar{D}_k &= \frac{D_k}{\gamma_z l_c^2}, & \bar{D}_z &= \frac{D_z}{\gamma_z l_c^2}, & \bar{D}_g &= \frac{D_g}{\gamma_z l_c^2}, \\
\bar{\mu}_b &= \frac{\mu_b}{\gamma_z}, & \bar{\mu}_g &= \frac{\mu_g}{\gamma_z}, & \bar{\beta}_k &= \frac{\beta_k R_{tot} K_{tot} \mu_b}{\gamma_z \alpha_b}, & \bar{\beta}_b &= \frac{\beta_b R_{tot}}{\gamma_z K_{tot}}, \\
\epsilon_1 &= \frac{\alpha_b}{\mu_b K_{tot}}, & \epsilon_2 &= \frac{\alpha_b}{\mu_b R_{tot}}, & \bar{\theta}_b &= \theta_b Z_{tot}, & \bar{\delta}_z &= \frac{\delta_z K_{tot}}{\gamma_z}, \\
\bar{\rho}_z &= \frac{\rho_z}{\gamma_z}, & \bar{\theta}_z &= \theta_z K_{tot}, & \bar{\beta}_z &= \frac{\beta_z \alpha_d}{\gamma_z \mu_d}, & \bar{\beta}_g &= \frac{\beta_g \alpha_g}{\gamma_z \mu_g}, \\
\bar{\gamma}_g &= \frac{\gamma_g}{\gamma_z}, & \bar{\mu}_r &= \frac{\mu_r}{\gamma_z}, & \bar{\lambda}^c &= \frac{\lambda^c}{\gamma_z}, & \bar{\lambda}^o &= \frac{\lambda^o}{\gamma_z}, \\
\bar{\beta}_d &= \frac{\beta_d \alpha_d}{\gamma_z \mu_d}, & \bar{\gamma}_d &= \frac{\gamma_d}{\gamma_z}, & \bar{\mu}_d &= \frac{\mu_d}{\gamma_z}, & \epsilon_3 &= \frac{\alpha_r \mu_d}{\mu_r \alpha_d}, \\
\epsilon_4 &= \frac{Z_{tot} \mu_d}{\alpha_d}, & \bar{\vartheta}_g &= \frac{\vartheta_g \mu_d^4}{\alpha_d^4}, & \epsilon_5 &= \frac{\alpha_r \mu_g}{\mu_r \alpha_g}, & \bar{\phi}_r &= \frac{\phi_r}{\gamma_z}, \\
\bar{\vartheta}_r &= \frac{\vartheta_r \mu_d}{\alpha_d}, & \bar{\phi}_d &= \frac{\phi_d}{\gamma_z}, & \bar{\vartheta}_d &= \frac{\vartheta_d \mu_d}{\alpha_d}.
\end{aligned}$$

Neglecting τ we write out the non-dimensionalised PDE-ODE system, with diffusion and hormone degradation occurring in the cytoplasm

$$\left. \begin{aligned} \frac{\partial b}{\partial t} &= D_b \partial_y^2 b - \mu_b b \\ \frac{\partial k}{\partial t} &= D_k \partial_y^2 k \\ \frac{\partial z_p}{\partial t} &= D_z \partial_y^2 z_p \\ \frac{\partial g}{\partial t} &= D_g \partial_y^2 g - \mu_g g \end{aligned} \right\} \text{in } \Omega_c. \quad (44)$$

Receptor binding and dissociation occurring on the plasma membrane

$$\left. \begin{aligned} -D_b \partial_y b &= \beta_k r_b k - \beta_b r_k b \\ -D_k \partial_y k &= \epsilon_1 (\beta_b r_k b - \beta_k r_b k) \\ -D_z \partial_y z_p &= 0 \\ -D_g \partial_y g &= 0 \\ \frac{dr_k}{dt} &= \epsilon_2 (\beta_k r_b k - \beta_b r_k b) \\ \frac{dr_b}{dt} &= \epsilon_2 (\beta_b r_k b - \beta_k r_b k) \end{aligned} \right\} \text{on } \Gamma_c. \quad (45)$$

The BR signalling processes occurring in the nucleus

$$\left. \begin{aligned} D_b \partial_y b &= \frac{\mu_b}{1 + (\theta_b z)^{h_b}} \\ D_k \partial_y k &= 0 \\ \frac{dz}{dt} &= \delta_z z_p k - \rho_z \frac{z}{1 + (\theta_z k)^{h_z}} - \beta_z z d_l + z_d \\ D_z \partial_y z_p &= -\delta_z z_p k + \rho_z \frac{z}{1 + (\theta_z k)^{h_z}} \end{aligned} \right\} \text{on } \Gamma_n. \quad (46)$$

The GA signalling processes occurring in the nucleus

$$\left. \begin{aligned} \frac{dr}{dt} &= -\beta_g r g + \gamma_g r_g^o + \mu_r (r_m - r) \\ \frac{dr_g^o}{dt} &= \beta_g r g - (\gamma_g + \lambda^c) r_g^o + \lambda^o r_g^c \\ \frac{dr_g^c}{dt} &= \lambda^c r_g^o - \lambda^o r_g^c - \beta_d d_l r_g^c + (\gamma_d + \mu_d) r_d \\ \frac{dr_d}{dt} &= \beta_d d_l r_g^c - (\gamma_d + \mu_d) r_d \\ \frac{dd_l}{dt} &= \epsilon_3 (-\beta_d d_l r_g^c + \gamma_d r_d) + \mu_d d_m - \epsilon_4 (\beta_z z d_l + z_d) \\ D_g \partial_y g &= \mu_g \frac{(d_l + \epsilon_4 \phi_z z)^4}{\vartheta_g + (d_l + \epsilon_4 \phi_z z)^4} - \epsilon_5 (\beta_g r g + \gamma_g r_g^o) \\ \frac{dr_m}{dt} &= \phi_r \left(\frac{d_l}{\vartheta_d + d_l} - r_m \right) \\ \frac{dd_l}{dt} &= \phi_d \left(\frac{\vartheta_d}{\vartheta_d + d_l} - d_m \right) \end{aligned} \right\} \text{on } \Gamma_n. \quad (47)$$

The crosstalk interactions occurring in the nucleus

$$\frac{dz_d}{dt} = \beta_z z d_l - z_d \quad \text{on } \Gamma_n. \quad (48)$$